HHS Public Access

Author manuscript

ACS Nano. Author manuscript; available in PMC 2021 July 12.

Published in final edited form as:

ACS Nano. 2020 May 26; 14(5): 5298–5313. doi:10.1021/acsnano.9b04926.

Surface Tethering of Inflammation-Modulatory Nanostimulators to Stem Cells for Ischemic Muscle Repair

Jiayu Leong,
Department of Chemical and Biomolecular Engineering, University of Illinois at Urbana–Champaign, Urbana, Illinois 61801, United States; Institute of Bioengineering and Nanotechnology, Singapore 138669 Singapore

Yu-Tong Hong,
Department of Chemical and Biomolecular Engineering, University of Illinois at Urbana–Champaign, Urbana, Illinois 61801, United States

Yu-Fu Wu,
Department of Kinesiology and Community Health and Beckman Institute for Advanced Science and Technology, University of Illinois at Urbana–Champaign, Urbana, Illinois 61801, United States

Eunkyung Ko,
Department of Bioengineering, University of Illinois at Urbana–Champaign, Urbana, Illinois 61801, United States

Svyatoslav Dvoretskiy,
Department of Kinesiology and Community Health and Beckman Institute for Advanced Science and Technology, University of Illinois at Urbana–Champaign, Urbana, Illinois 61801, United States

Jye Yng Teo,
Department of Chemical and Biomolecular Engineering, University of Illinois at Urbana–Champaign, Urbana, Illinois 61801, United States; Institute of Bioengineering and Nanotechnology, Singapore 138669 Singapore

Byoung Soo Kim
Department of Chemical and Biomolecular Engineering, University of Illinois at Urbana–Champaign, Urbana, Illinois 61801, United States

Kyeongsoo Kim, **Hojeong Jeon**

Corresponding Author: Hyunjoon Kong – *Department of Chemical and Biomolecular Engineering, Beckman Institute for Advanced Science and Technology, Department of Bioengineering, and Carl R. Woese Institute for Genomic Biology, University of Illinois at Urbana–Champaign, Urbana, Illinois 61801, United States; Department of Medical Engineering, Yonsei University College of Medicine, Seoul 03722, Republic of Korea;* hjkong06@illinois.edu.

Complete contact information is available at: https://pubs.acs.org/10.1021/acsnano.9b04926

The authors declare no competing financial interest.

Supporting Information

The Supporting Information is available free of charge at https://pubs.acs.org/doi/10.1021/acsnano.9b04926.

Additional methods for the synthesis of HA-*g*-C18, kinetic analysis of liposome tethering to ADSC surface, preparation of TNFα-releasing HA-liposomes with different TNFα concentrations, kinetic release of TNFα from liposomes, quantification of VEGF, PEDF, and PGE_2 in the presence of anti-TNFα antibodies, fabrication of microfluidic device, quantification of VEGF and PEDF from muscle tissues, and histological analysis of muscle tissues, equations for FRET analysis and the kinetic analysis of liposome tethering to the ADSC surface, and Figures S1 to S11 (PDF)

Center for Biomaterials, Biomedical Research Institute, Korea Institute of Science and Technology, Seoul 02792, Republic of Korea

Marni Boppart,
Department of Kinesiology and Community Health and Beckman Institute for Advanced Science and Technology, University of Illinois at Urbana–Champaign, Urbana, Illinois 61801, United States

Yi Yan Yang,
Institute of Bioengineering and Nanotechnology, Singapore 138669 Singapore;

Hyunjoon Kong
Department of Chemical and Biomolecular Engineering, Beckman Institute for Advanced Science and Technology, Department of Bioengineering, and Carl R. Woese Institute for Genomic Biology, University of Illinois at Urbana–Champaign, Urbana, Illinois 61801, United States; Department of Medical Engineering, Yonsei University College of Medicine, Seoul 03722, Republic of Korea;

Abstract

Stem cell transplantation has been a promising treatment for peripheral arterial diseases in the past decade. Stem cells act as living bioreactors of paracrine factors that orchestrate tissue regeneration. Prestimulated adipose-derived stem cells (ADSCs) have been proposed as potential candidates but have been met with challenges in activating their secretory activities for clinical use. Here, we propose that tethering the ADSC surface with nanoparticles releasing tumor necrosis factor α (TNFα), named nanostimulator, would stimulate cellular secretory activity *in situ*. We examined this hypothesis by complexing octadecylamine-grafted hyaluronic acid onto a liposomal carrier of TNFα. Hyaluronic acid increased the liposomal stability and association to CD44 on ADSC surface. ADSCs tethered with these TNFα carriers exhibited up-regulated secretion of proangiogenic vascular endothelial growth factor and immunomodulatory prosteoglandin E2 (PGE_2) while decreasing secretion of antiangiogenic pigment epithelium-derived factors. Accordingly, ADSCs tethered with nanostimulators promoted vascularization in a 3D microvascular chip and enhanced recovery of perfusion, walking, and muscle mass in a murine ischemic hindlimb compared to untreated ADSCs. We propose that this surface tethering strategy for *in situ* stimulation of stem cells would replace the costly and cumbersome preconditioning process and expedite clinical use of stem cells for improved treatments of various injuries and diseases.

Graphical Abstract

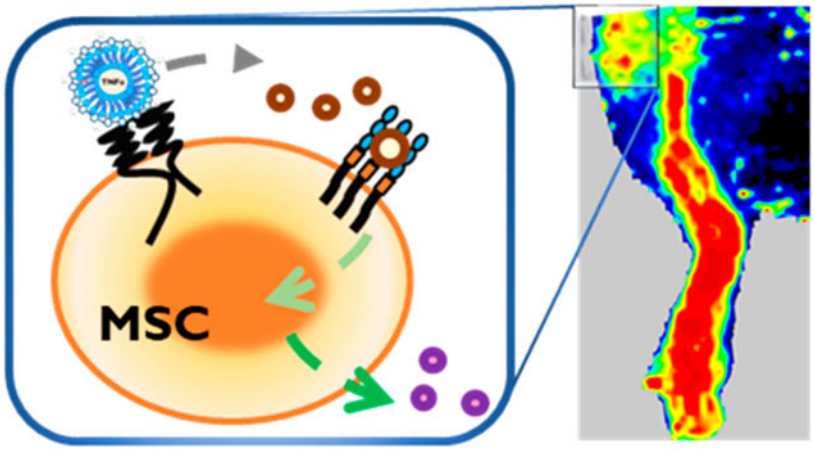

Keywords

angiogenesis; adipose-derived stem cells; hyaluronic acid; vascular endothelial growth factor; muscle; liposome

Adipose-derived stem cells (ADSCs) have emerged as a new generation of medicine that can repair ischemic tissues stemming from vascular rupture or occlusion.[1] ADSCs secrete multiple paracrine growth factors and cytokines that orchestrate recruitment, proliferation, and differentiation of tissue-forming host cells, while alleviating inflammation and cell death.[2] For instance, ADSCs secrete both proangiogenic factors (*e.g.*, vascular endothelial growth factor (VEGF) and monocyte chemoattractant protein-1) and antiangiogenic pigment epithelium-derived factor to regulate endothelial sprouting and maturation.[3,4] ADSCs also secrete immunomodulatory factors, such as prostaglandin E2 (PGE_2). PGE_2 inhibits dendritic cell differentiation and maturation and promotes the generation of immunosuppressive regulatory T cells.[5,6] As a result, transplanted ADSCs support the tissue recovery process by preventing the escalation of infiltrating leukocytes that release reactive oxygen species and contribute to the inflammatory environment.[7] Furthermore, ADSCs have been found to evade allogenic rejection, which allows patients to receive cells from matching donors.[8–10]

In the past, cell therapies were conducted by administering the media collected from the ADSC culture *in vitro*. Recently, preclinical trials increasingly adopt intramuscular cell injection for enhanced therapeutic outcome.[11] Success in the cell therapy therefore relies on the ability of cells to secrete desired therapeutic molecules in a sustainable manner. To meet this requirement, cells are activated with media supplemented with cytokines that normally initiate repair processes. For example, infusion of mesenchymal stem cells preconditioned with transforming growth factor-alpha or platelet-derived growth factor-BB enhanced the recovery of hearts inflicted with acute myocardial ischemia/reperfusion injury.[12,13] In these studies, the soluble factors activate the mitogenic signal transduction pathways to induce the production of growth factors such as VEGF. Separately, ADSCs preconditioned with tumor necrosis factor alpha (TNFα) activated the expression of proangiogenic genes and promoted growth of capillaries *in vitro*.[14] It is common to plate cells in a cell culture flask, incubate

them in media supplemented with stimulatory cytokines over 24 to 48 h, and finally detach them from the flask. This process is labor-intensive and costly. Also, depending on the cell culture media formulation, cells may be exposed to immunogens in serum.

In addition, it is unclear whether the preconditioned ADSCs remain active throughout the treatment period.[15,16] This concern motivated efforts that aim to transduce cells with viral vectors containing genes for hypoxia-inducible factor and insulin-like growth factor, so as to make cells secrete the proteins continuously.[17–19] However, the long-term safety of genetically engineered stem cells is still unknown, thus acting as a potential obstacle to clinical translation. Additionally, other factors including cell culture media composition during the *ex vivo* culture also raise concerns about the immunogens, labor, and costs.[20–23]

In order to improve the therapeutic efficacy of transplanted stem cells, it would be desirable to develop a method that can stimulate cellular secretion activity *in situ* while circumventing concerns about safety and immunogenicity resulting from the preconditioning method. To this end, we hypothesize that ADSCs tethered with liposomes encapsulating TNFα, referred to as the "nanostimulator", would display sustained secretion activity in a transplanted site. TNFα is an inflammation cytokine and has been used as an angiogenic inducer in the preconditioning of ADSCs. This cytokine modulates tissue regeneration, including angiogenesis and extracellular matrix remodeling.[24] However, the stimulatory efficacy of TNFα depends on the dose. High levels of TNFα can induce apoptosis of MSCs and hence reduce their secretion activities.[25] Therefore, it is critical to keep the concentration of TNFα at a level appropriate to stimulate the cellular secretion activity. We propose that temporally continued release of TNFα from the liposomes on the cell surface would activate signaling pathways responsible for cell secretion and, in turn, stimulate cellular secretion activity without the need for preconditioning. This strategy would significantly improve the activation of transplanted ADSCs to restore perfusion and strength of ischemic muscles.

To examine this hypothesis, we assembled the nanostimulator by loading TNFα into the liposomes coated with hyaluronic acid that binds with CD44 of ADSCs (Scheme 1). The diameter of liposomes was kept constant at 400 nm to minimize cellular uptake of liposomes. First, we examined the binding kinetics and residence of the nanostimulator on the surface of ADSCs. Second, we analyzed secretion profiles of ADSCs modulated by the nanostimulator, particularly secretion of proangiogenic VEGF, antiangiogenic PEDF, and immunomodulatory PGE_2, along with the underlying signaling cascade. Then, we examined the extent that the nanostimulator enhances paracrine activity of MSCs toward neovascularization using a microfluidic chip assembled to recapitulate angiogenesis. Finally, we tested the therapeutic efficacy of the ADSCs tethered with the inflammation-modulatory nanostimulator by transplanting them into a mouse ischemic hindlimb model and monitoring the rate of perfusion recovery and the retention of muscle physiology.

RESULTS AND DISCUSSION

Assembly of Nanostimulator, an ADSC-Adherent Liposomal Carrier of TNFα.

Hyaluronic acid (HA) binds to ADSC surface receptors CD44 and CD168, similar to the natural HA responsible for homeostasis and tissue regeneration.[26] In particular, we used HA

with a molecular weight of 100 kDa to enhance binding to cells. As a flexible polymer, HA forms a swollen random coil in dilute aqueous solution. HA with a molecular weight of 100 kDa would have a radius of gyration of 21 nm[27] and binds to more than one CD44.[28,29] To associate with liposomes, HA was alkylated by forming an amide bond between octadecylamine and glucuronic acid monomers of hyaluronic acid, catalyzed by 1-ethyl-3-(3-(dimethylamino)propyl)carbodiimide and *N*-hydroxysuccinimide. The presence of octadecyl chains on hyaluronic acid was confirmed by the presence of the triplet at 0.85 ppm on the ^{1}H NMR spectroscopy spectrum, assigned to the protons on the terminal carbon of octadecylamine (Figure S1). The degree of substitution was calculated to be 3% by taking the ratio of CH_3 between octadecylamine and glucosamine groups. The resulting alkyl-substituted hyaluronic acid, termed HA-*g*-C18, is soluble in cell culture media supplemented with 10% serum.

Liposomes coated with HA-*g*-C18 were prepared by hydrating a thin film of lipid molecules followed by vigorous mixing of resulting liposomes with HA-*g*-C18. HA-*g*-C18 and lipid molecules were labeled with rhodamine B and nitrobenzoxadiazole, respectively. The confocal image shown in Figure 1A displayed the colocalization of fluorescence from HA-*g*-C18 and the lipid bilayer. In contrast, the liposome mixed with unmodified HA presents a lower fluorescence of rhodamine B than that mixed with HA-*g*-C18 (Figure S2A).

The role of octadecyl chains of HA-*g*-C18 on increasing binding affinity between HA and liposome was examined with the fluorescence resonance energy transfer (FRET) between rhodamine B (FRET acceptor) on HA and nitrobenzoxadiazole on the liposome (FRET donor). Upon excitation at a wavelength of 420 nm, an absorption wavelength of nitrobenzoxadiazole, the aqueous mixture of HA-*g*-C18 and liposomes displayed a decreased emission intensity of nitrobenzoxadiazaole maximized at 530 nm, compared with the emission intensity of the liposome free of HA-*g*-C18 (Figure 1B). Also, the mixture of liposome and HA-*g*-C18 showed the increased emission intensity of rhodamine B maximized at 590 nm compared with the aqueous solution of HA-*g*-C18. Both the decrease of the FRET donor emission intensity and the increase of the FRET acceptor emission intensity indicate the close proximity of HA and liposomes. The FRET efficiency, calculated using eq S1 was 22%. In contrast, the aqueous mixture of unmodified hyaluronic acid and liposomes exhibited an increase of the emission intensity of rhodamine B maximized at 590 nm, but the FRET efficiency, being 13%, was lower than that of the mixture of HA-*g*-C18 and liposomes (Figure 1C).

The resulting liposomes coated with HA-*g*-C18, denoted as HA-liposome, were resized to nanosized particles by extruding them through a 400 nm pore diameter membrane. The diameters of the liposomes were uniformly 400 nm, as confirmed with a dynamic light scattering unit (Figure S2B). The zeta potential of unmodified liposomes was 5 mV, while that of the liposome coated with HA-*g*-C18 was −36 mV, regardless of the diameter (Figure S2C). 1,2-Dipalmitoyl-*sn*-glycero-3-phosphocholine exists as a zwitterionic form and confers the liposomes formed with a net neutral charge. In contrast, glucuronic acid of HA has a pK_a of 3.2 and is therefore deprotonated to present a negative charge in DI water. Due to the negative zeta potential, the HA liposomes remained more stable in aqueous media than unmodified liposomes without aggregation nor sedimentation. In blood-mimicking

media containing serum albumin, HA liposomes remained stable for at least 24 h, while unmodified liposomes fused immediately to form particles of greater than 1 μm (Figure 1D,E).

TNFα was loaded into the liposomes by mixing them into the hydration medium used to form the liposomes. The encapsulation efficiency of TNFα loaded in unmodified liposomes and HA liposomes coated with HA-*g*-C18 (HA-liposomes) was 73% and 83%, respectively (Figure S3A). The release profile of TNFα from HA-liposomes showed a sustained and steady release over 5 days of incubation in neutral media at 37 °C (Figure S3B). Fifteen percent of the loaded TNFα was released initially from HA-liposomes. In contrast, the release profile of the unmodified liposomes followed a biphasic profile. There was an initial burst release of the loaded TNFα (55%) likely due to the unstable aggregation of liposomes shown in Figure S3C.

The TNFα release profiles were fit against the empirical model describing the fractional release at time t, $\frac{\text{Cumulative mass of TNF}\alpha\text{ released at time, } t}{\text{Total mass of TNF}\alpha\text{ released}} = kt^n$ (Figure S3D). In the equation, k represents the release rate constant and n represents the release exponent. n for HA-liposomes was 0.42, which indicates that liposomes released TNFα mainly by diffusion from t = 8 to 120 h (Figure S3E).[30] In contrast, n of the unmodified liposomes was 0.20, which may be attributed to the polydispersed size distribution. The k value for unmodified liposomes was 7-fold higher than that of HA liposomes, indicating that the HA-*g*-C18 coating reduced the rate of TNFα release (Figure S3F).

Kinetic Analysis of the Liposomes Tethering to ADSC Surface.

We assessed the extent that HA immobilized on the liposome modulates the number of liposomes tethered to ADSCs using the liposomes labeled with nitrobenzoxadiazole. Cells were incubated in the suspension of unmodified liposome or HA liposomes for 15 min while gently shaking the mixture at 37 °C. According to the confocal images of cells captured after removing nonadherent liposomes, cells that were incubated with HA liposomes yielded a larger fluorescence than cells incubated with unmodified liposomes (Figure 2A). In parallel, the number of liposomes tethered to cells was counted with fluorescence spectroscopy. The number of unmodified liposomes per cell was 58 000, while that of HA liposomes was 94 000 (Figure 2B).

To estimate the equilibrium dissociation constant, K_D, the ADSCs were incubated with different concentrations of nitrobenzoxadiazole-labeled liposomes and the number of surface-tethered liposomes at equilibrium was measured (Figure 2C, eq S2). HA-liposomes associated with ADSCs at a higher affinity than unmodified liposomes. K_D of HA liposomes was 93 pM, while that of unmodified liposomes was 231 pM. In addition, the dissociation rate constant, k_{-1}, was measured by placing ADSCs with surface-tethered liposomes in fresh media and counting the number of liposomes remaining on the cell surface at various time points (eq S3). The k_{-1} of the HA-liposomes was 0.0091 min^{-1}, while that of unmodified liposomes was 0.013 min^{-1}. As a result, the time required for half the HA-liposomes to dissociate from the surface ($t_{1/2}$), calculated using eq S4, was 76 min. In contrast, $t_{1/2}$ of the unmodified liposomes was 53 min. The multivalent interactions between HA-liposome and

multiple receptors on the cell were shown to drastically increase in the binding stability as shown in Figure 2B and C(iii). Therefore, in comparison to unmodified liposomes, the HA molecules on the liposomal surface serve to increase the number of liposomes bound to the ADSCs. Unmodified liposomes adhered to cells minimally by nonspecific interactions and sediment quickly. We also propose that the resulting HA-liposome would be readily usable in a clinical setting and retain biological activity of cells, although the adhesion strength of particles may have to be increased further.[31,32]

To determine if the ADSCs suspended in media took up HA-liposomes, intracellular lysosomes were labeled with Lysotracker Green. Separately, HA-*g*-C18 on the surface of liposomes were chemically coupled with rhodamine B. If the cells took up the liposomes, there should be colocalization of fluorescence signals from both liposomes and lysosomes. HA-liposomes were found only on the cell surface after incubating cells in suspension for 2 h (Figure 3A). This result is because mesenchymal stem cells are nonphagocytic cells.[33] Then, cells were seeded on a type I collagen gel to simulate cells transplanted in tissue. After 24 h, most of the HA-liposomes were found on the cell surface as confirmed with minimal colocalization of fluorescence from liposomes and lysosomes (Figure 3B). There was no significant cellular uptake of HA-liposomes even after 3 days and 5 days of incubation (Figure S4).

In Vitro Analysis of the Stimulatory Function of TNFα-Releasing HA-Liposomes.

Next, TNFα-carrying HA-liposomes were assessed for their ability to stimulate cells to secrete factors in a pseudoautocrine fashion. The critical TNFα loading mass to activate ADSCs was 2500 ng per mg liposome (Figure S5). The HA-liposomes tethered to ADSCs circumvent the dependency of endogenously produced TNFα to activate the ADSCs.[34] Also, effective paracrine signaling *in vivo* requires close proximity of stem cells to the cytokine-secreting cells such as T cells.[35,36] Previous studies estimated that stimulated T cells secrete an average of two TNFα molecules per second but this diminished over 12 h.[37] Also, cytokines secreted from T cells diffuse and peak at about four cells away. As a consequence, the TNFα concentration is drastically diluted by diffusion in the three-dimensional tissue.[38] In contrast, we propose that the TNFα-releasing HA-liposomes tethered to stem cells can reduce the proximity of TNFα to the TNF receptors and, in turn, amplify the efficacy of TNFα. In addition, continued release of TNFα from the HA-liposomes on the cell surface enabled ADSCs to keep an activated state for secretion of proangiogenic factors including VEGF and immunomodulatory factors including PGE_2. TNFα does not stimulate cellular uptake of the liposomes.[39]

The secretion profile of the ADSCs activated by the TNFα-releasing liposomes was examined with an array of antibodies toward angiogenesis-related proteins (Figure 4). During 24 h of cell culture on the type I collagen gel, ADSCs released a series of proangiogenic factors, activin A, angiogenin, interleukin-8 (IL-8), monocyte chemoattractant protein 1 (MCP-1), and VEGF, and antiangiogenic factors, pigment epithelium-derived factor (PEDF). The cells also secreted inhibitors such as tissue inhibitor of metalloproteinase-1 (TIMP-1) and plasminogen activator inhibitor (PAI-1), which decrease remodeling and fibrosis, respectively. Additionally, the cells released antiapoptotic

cytokines insulin-like growth-factor-binding protein 3 (IGFBP-3), pentraxin-related protein (PTX-3), thrombospondin-1 (TSP-1), and urokinase plasminogen activator (uPA).

The continued presence of activating cytokines such as TNFα is essential for continued cellular secretion activities because the stimulatory effects of TNFα are inherently short-lived.[40,41] However, the reparation of tissues transpires on longer time scales. Thus, we propose that the continual TNFα release would prolong the activation of transcription of therapeutic molecules *via* the sustained activation of the associated signaling pathways.

The secretion levels of proangiogenic VEGF, antiangiogenic PEDF, and immunomodulating PGE_2 were measured using ELISA for individual proteins. On day 1, the VEGF secretion level of ADSCs tethered with TNFα-releasing HA-liposomes was 1.7-fold higher than untreated ADSCs (Figure S6A). VEGF secretion from an initial seeding of 10 000 cells was sustained and reached 3 ng mL^{-1} after 5 days (Figure 5A). The VEGF secretion level of ADSCs tethered with TNFα-releasing HA-liposomes was 1.9-fold higher than the untreated ADSCs, ADSCs preconditioned with free TNFα, and ADSCs mixed with blank unmodified liposomes.

To determine the mechanism for activating VEGF up-regulation, ADSCs were incubated with inhibitors to VEGF transcription regulators, including extracellular signal-regulated kinases (ERK) and p38 mitogen-activated protein kinases (MAPK). The inhibitors had minimal effects on the untreated ADSCs. In contrast, for ADSCs tethered with TNFα-releasing HA-liposomes, the MAPK inhibitor suppressed the VEGF secretion level more significantly than the ERK inhibitor (Figure 5B).

The secretion levels of antiangiogenic PEDF by ADSCs continued to increase to 40 ng mL^{-1} over 5 days of culture (Figure 5C).[42] No difference of the secretion level was found among untreated ADSCs, ADSCs preconditioned with free TNFα, ADSCs mixed with unmodified liposomes, and ADSCs tethered with blank HA-liposomes (Figures S6B and 5). In contrast, the ADSCs tethered with TNFα-releasing HA-liposomes exhibited a 1.2-fold lower secretion level of PEDF.

Immunomodulatory PGE_2 is a potent mediator responsible for immunosuppression and anti-inflammation by ADSCs.[43] ADSCs tethered with TNFα-releasing HA-liposome displayed 2-fold higher PGE_2 secretion than other conditions including untreated ADSCs, ADSCs mixed with unmodified liposomes, and ADSCs tethered with blank HA-liposomes (Figure 5D). After 48 h, the PGE_2 secretion level was approximately 9 ng mL^{-1}. There was no significant difference in the concentration of secreted VEGF, PEDF, and PGE_2 between untreated ADSCs and ADSCs tethered with TNFα-releasing HA-liposomes in the presence of anti-TNFα antibodies (Figure S7). This is because the anti-TNFα antibodies form a TNFα–antibody complex that prevents TNFα from binding to TNFα receptors on ADSCs and, consequently, the anti-TNFα antibodies nullify the stimulatory effect of TNFα. This result confirms that TNFα released from the tethered HA-liposomes regulates cellular secretion activities by binding with TNFα receptors of the cell, as shown in Figure 4.

Subsequent studies then focused on analyzing the therapeutic activities of ADSCs tethered with TNFα-releasing HA-liposomes in comparison to untreated ADSCs. The therapeutic

efficacy of the activated ADSCs to induce angiogenesis was assessed with a 3D microvascular device assembled for *in vitro* neovascularization study (Figure 6A).[44] The microfluidic system used herein is advantageous over the typical microwell plate assay, which relies on a basement membrane that inherently contains a small amount of growth factors capable of inducing premature tube formation. Also, endothelial tubes formed on the matrix detach and break apart quickly after 16–24 h, which undermines a long-term evaluation of the role of stem cells on vascularization. In contrast, using the microfluidic system, we observed the stable formation of tubule networks over 5 days. Additionally, the microfluidic platform separates endothelial cells from ADSCs using a channel filled with media to mimic the initial spatial separation upon cell transplantation.

Human umbilical vein endothelial cells (HUVECs) as vascular precursor cells were seeded in a fibrin gel that filled the central channel (Figure 6B). ADSCs were seeded in a fibrin gel that filled the outer channels. Thus, bioactive molecules released from ADSCs diffuse into the central channel in which HUVECS reside. In the absence of ADSCs, HUVECs aggregated to form cell clusters (Figure 6C). In the presence of untreated ADSCs, HUVECs formed hollow endothelial lumens, which were interconnected to each other. ADSCs tethered with TNFα-releasing HA-liposomes resulted in endothelial lumen, which is interconnected more compactly than untreated ADSCs. The tubule length was increased by 1.3-fold with ADSCs tethered with TNFα-releasing HA-liposomes, compared with untreated ADSCs (Figure 6D). The number of interconnected junctions was 1.3-fold greater with ADSCs tethered with TNFα-releasing HA-liposomes than untreated ADSCs (Figure 6E).

In Vivo Assessment of Therapeutic Efficacy of ADSCs to Treat Ischemic Hindlimb.

Finally, the therapeutic efficacy of ADSCs tethered with TNFα-releasing HA-liposomes was evaluated *in vivo* by using an ischemic hindlimb model introduced into outbred CD-1 mice (Figure 7A). The ligation of the right femoral artery and vein resulted in impaired perfusion, as confirmed with laser Doppler perfusion imaging (LDPI) (Figure 7B). In contrast, the left intact hindlimb retained normal perfusion, the same as the mouse that did not undergo vascular ligation. The PBS solution, untreated ADSCs, or ADSCs tethered with TNFα-releasing HA-liposomes were injected into the tibialis anterior and gastrocnemius muscle immediately after vascular ligation.

According to the LDPI measurements, on the first day after the ischemic injury was induced, the mice from all experimental groups had an average perfusion ratio of 0.14, which is quantified as the ratio of perfusion between the right ischemic hindlimb and the left intact hindlimb. Subsequently, on day 7, the mice transplanted with ADSCs tethered with TNFα-releasing HA-liposomes displayed a 2-fold increase in the average perfusion ratio to 0.62 compared to mice that received PBS (Figure 7C). The average perfusion ratio of mice transplanted with ADSCs tethered with TNFα-releasing unmodified liposomes remained at 0.34, similar to mice that received PBS and untreated mice. The perfusion level remained similar on day 14 and comparable to preconditioned ADSCs (Figure S8).

We further examined the extent of the areal density of blood vessels in increasing blood perfusion. We examined the vascular density 14 days after injecting ADSCs or ADSCs

tethered with TNFα-releasing HA liposomes. For this analysis, we focused on the lower limb muscles, which were known to be affected the most by the ischemic injury, in comparison to the thigh muscles, which recover more quickly due to collateral artery formation.[45,46] Both the tibialis anterior and the gastrocnemius muscle, where the cells were injected, were isolated and stained with antibodies against CD31 and alpha smooth muscle actin (αSMA). CD31 and αSMA represent the endothelium and the smooth muscle or pericyte layer formed on mature, moderate-sized blood vessels, respectively (Figure 8A(i)). The average number of capillaries found in the tibialis anterior was 1303 per square millimeter of muscle (Figure 8A(ii)). This is 1.2 times higher than the tibialis anterior that was transplanted with untreated ADSCs. Gastrocnemius muscle that was transplanted with ADSCs tethered with TNFα-releasing liposomes had an average of 34 arterioles per square millimeter of muscle (Figure 8B(i) and (ii)). This is 1.5 times more than gastrocnemius muscles that received only PBS. There was no significant difference between muscles that were transplanted with untreated ADSCs and muscles that received only PBS. There was no significant difference in the number of capillaries per square millimeter among the three groups (Figure 8B(iii)).

Compared to muscles that were injected with PBS, the muscles injected with ADSCs tethered with TNFα-releasing HA liposomes had fewer macrophages (Figure S9), indicating that the transplantation of activated stem cells did not pose any long-term inflammatory effects.

The extent of the injection site in affecting the therapeutic efficacy of the ADSCs was examined. Directing the cells into an upstream muscle such as the quadriceps also minimizes additional injury to the muscle from the injection needle, which could confound our analysis. PBS solution, untreated ADSCs, or ADSCs tethered with TNFα-releasing HA-liposomes were injected into the quadriceps and gastrocnemius muscle immediately after vascular ligation. Similarly, according to the LDPI measurements, on the first day after the ischemic injury was induced, the mice from all experimental groups had an average perfusion ratio of 0.15, which was quantified as the ratio of perfusion between the right ischemic hindlimb and the left intact hindlimb. Subsequently on day 7, the mice transplanted with untreated ADSCs displayed a 2-fold increase in the average perfusion ratio to 0.56 compared to mice that received PBS (Figure S10). However, the average perfusion ratio of mice transplanted with untreated ADSCs remained the same at 0.51 through the following 3 weeks. The average perfusion ratio on day 28 was similar to that of mice injected with PBS. In contrast, the ADSCs tethered with TNFα-releasing HA-liposomes served to increase the average perfusion ratio to 0.70 within 7 days. The perfusion level remained stable at a value of 0.75 until the 28th day. Therefore, we found that the choice of injection sites for cell transplantation, whether splitting between the upper and lower limb or entirely in the lower limb, may affect the therapeutic efficacy of cells. The significance of the effects of an injected site and subsequently altered transport routes of cell-secreting factors will be examined more thoroughly in a following study.

We further quantified the mean walking stride length of the mice at day 26 (Figure 9A). Mice treated with PBS or untreated ADSCs had a similar stride length of 5.9 cm (Figure

9B). In contrast, mice treated with ADSCs tethered with TNFα-releasing HA-liposomes had a stride length of 6.8 cm, which is similar to mice without vascular ligation surgery.[47–49]

Mouse hindlimb strength was evaluated by electrically stimulating the muscle fibers in the hindlimb and measuring the isometric contraction torque *in vivo* on the last day of the studies, day 14 and day 28, respectively. For both studies, there were no significant differences among the experimental groups where the mean maximum isometric torque was 285 and 383 N·mm kg^{-1}, respectively (Figure 10A). On the other hand, there was a significant 1.2-fold increase in gastrocnemius muscle mass (Figure 10B) in mice transplanted with ADSCs tethered with TNFα-releasing HA-liposomes.

Although the limb ischemia in humans and animal models elevates the levels of VEGF and other angiogenic cytokines, the elevated level is not sufficient or sustained for the full recovery from the standpoints of perfusion and muscle strength.[50] Also, efforts are increasingly made to administer multiple growth factors that augment angiogenesis and vascular maturation.[51,52] In this regard, we suggest that stem cells tethered with nanostimulators could sustain stable angiogenic activity and immunomodulatory activity. Specifically, the VEGF secreted by ADSCs sustainably would initiate the host endothelial cells to form blood vessel tubules. The PEDF still secreted by cells over the course of recovery could facilitate stabilization of blood vessels to vascularize the ischemic limb. There was a 1.3-fold higher VEGF level found in the muscle where ADSCs tethered with TNFα-releasing liposomes were transplanted than in the muscle where PBS or untreated ADSCs were transplanted (Figure S11). The levels of PEDF found in the muscles of all groups were similar. Overall, these cell-secreting factors contributed to making a marked increase in perfusion within 7 days, thus preventing deterioration of locomotion and mass of muscle following the ischemic injury.

Besides releasing therapeutic angiogenic factors to facilitate perfusion recovery, other ADSC-secreting bioactive molecules might have influenced ischemic muscle recovery. In particular, anti-inflammatory molecules such as PGE_2 might have limited an abnormal increase of cellular oxidative stress and subsequent death of host cells responsible for tissue repair and regeneration. In addition, TNFα released from HA-liposomes on ADSCs did not activate the proliferation of ADSCs, which can increase the probability of mutation. Finally, previous studies reported that TNFα also limits undesired cell differentiation,[53] which will be examined thoroughly in future studies.

In this study, ischemic injury introduced in the mice did not lead to a significant reduction in muscle strength compared with intact hindlimbs. This result is probable because there was no severe venous trauma or neuropathy intentionally induced nor were the muscles subjected to extreme stresses post-injury.[54,55] Furthermore, these mice have an ability to recover perfusion up to 40% without any treatment.[56] As a proof-of-concept, our *in vivo* model accounts for only a basic form of ischemic limb. However, the added complexities of other underlying diseases would have to be carefully selected, as it is still a challenge to replicate similar severity on animal models.[57] We envisage that the efficacy of activated stem cells to prevent deterioration of muscle strength would be more significant with diabetic, aged, or stressed mice models with less self-healing capability.[58–60] In addition, we have

demonstrated that the transplantation of activated ADSCs is safe in the presence of a normal immune system that would respond to allogeneic cells. However, whether the transplanted ADSCs die or disappear following the treatment should be examined carefully in future studies.

Also, the results of this study have outlined a simpler and less manipulative procedure to stimulate stem cells than the current ones reported in the literature. Specifically, the FDA has defined a minimal manipulation process performed on the cells should not alter the biological characteristics of the cells.[61] To comply with this requirement, this study utilized recombinant TNFα as a stimulant because the molecule can activate stem cells in the same way as endogenous TNFα. Compared to efforts to genetically modify stem cells, the stimulation with TNFα is less manipulative and will be more acceptable to patients. Therefore, the use of nanostimulants that adhere to stem cells and release TNFα cargos could be easily integrated into various stem cell therapies to treat acute injuries and graft *versus* host disease. In addition, the strategy can be readily translated into clinical treatments. For example, clinicians can mix the premade nanostimulators with stem cells and inject the cell–nanostimulator mixture into the target tissue without plating cells on a cell culture flask for preconditioning. Therefore, cells isolated from a patient's adipose tissue do not have to leave the operation room. By doing so, this strategy would circumvent any potential contamination during preconditioning.

The adhesion of the HA-liposomes to the cell surface was attained by the natural HA ligand–CD44 receptor bond as well as nonspecific interactions, including hydrogen bonding.[62] The liposomes tethered onto the cells may detach from the cells by interstitial fluid flow within the transplanted muscle. The fluid exerts shear force on the cell membrane. The mechanical force exerted by neighboring muscle contraction may be another factor to drive the separation of liposomes from the cell. To prevent this problem, HA-liposomes will be modified with additional biochemical cues that can bind with integrins of stem cells more strongly and increase the adhesion strength to the cells in future studies.

CONCLUSION

Taken together, we conclude that the *in situ* stimulation of adipose-derived stem cells by tethering nanostimulators is a promising strategy to activate and sustain secretory activity and, in turn, improve therapeutic efficacy of ADSCs. The HA-liposome used as a model, stem cell-adherent nanocarrier of TNFα adhered to stem cells by recapitulating a mechanism by which natural HA binds to hyaluronan receptors of cells. The stem cells tethered with these TNFα-releasing HA-liposomes displayed markedly increased secretory activities likely because of continuous binding of TNFα to TNFα receptors and activation of MAPK signal pathways. As a consequence, stem cells tethered with the nanostimulators served to improve neovascularization and perfusion recovery and finally prevent muscle loss following acute ischemic injury in the hindlimb. We envisage that the nanostimulator would replace the preconditioning process, thus making stem cell transplantation therapy simple and effective for challenging medical problems. Furthermore, differentiation-promoting factors or small molecules may also be encapsulated in the nanostimulator to regulate phenotypes of differentiated cells and, in turn, promote tissue regeneration.

MATERIALS AND METHODS

Synthesis of HA-*g*-C18.

Sodium hyaluronate (FMC BioPolymer) (100 mg, 0.25 mmol of −COOH) was dissolved in formamide (5 mL) by sonication for 30 min and gentle heating. After the solution was cooled to room temperature, a two molar excess of 1-ethyl-3-(3-(dimethylamino)propyl)carbodiimide hydrochloride (96 mg) and *N*-hydroxysuccinimide (58 mg) were added and stirred for 2 h to activate the carboxylic group. Then, octadecylamine (3.6 mg, 12.5 μmol) dissolved in anhydrous DMF (1 mg mL^{-1}) was added slowly to the solution. To label hyaluronic acid with rhodamine B, lissamine rhodamine B ethylenediamine (1.6 mg dissolved in DMSO, 50 mg mL^{-1}; Invitrogen) was added to the reaction mixture. Then, the reaction mixture was stirred at 60 °C under a nitrogen atmosphere for 5 h and an additional 24 h at room temperature. The resultant mixture was dialyzed against an excess amount of water/ethanol for 2 days and distilled water for another 2 days. Finally, the solution was filtered with a 0.45 μm filter to remove other impurities, followed by lyophilization. The modified HA is referred to as HA-*g*-C18. To determine the degree of substitution by ^{1}H NMR analysis, HA-*g*-C18 was dissolved in deuterium oxide (Cambridge Isotope Laboratory) at a concentration of 10 mg mL^{-1}. ^{1}H NMR (500 MHz, D_2O, 22 °C): δ 3.3–4.0 (m, hyaluronic acid sugar backbone), 3.2 (m, $CH_2(CH_2)_{16}CH_3$), 2.9 (m, $CH_2(CH_2)_{16}CH_3$), 2.05 (s, −$COCH_3$ of hyaluronic acid), 0.85 (t, $CH_2(CH_2)_{16}CH_3$).

Liposome Preparation.

Liposomes were prepared by a film hydration method followed by vortex mixing and extrusion. 1,2-Dipalmitoyl-*sn*-glycero-3-phosphocholine (DPPC; Avanti Polar Lipids) was dissolved with chloroform at a concentration of 10 mg/mL in a round-bottom flask. Chloroform was removed by rotary evaporation to form a thin lipid film. The film was then hydrated with HA-*g*-C18 dissolved in deionized water (2 mg mL^{-1}) at 50 °C, which is above the transition temperature of DPPC. The lipid concentration was kept constant at 1 mg mL^{-1}. For experiments involving fluorescently labeled liposomes, referred to as NBD-liposomes, 0.002 mg of 1-palmitoyl-2-{12-[(7-nitro-2–1,3-benzoxadiazol-4-yl)amino]-dodecanoyl}-*sn*-glycero-3-phosphocholine) (Avanti Polar Lipids) was mixed with 1 mg of DPPC. The mixture was immediately vortexed for 30 s and extracted into a glass syringe. The liposomes were sized down by passing the liposome suspension 21 times through a 400 nm polycarbonate membrane assembled on the Avanti mini extruder. For experiments involving encapsulation of TNFα, TNFα (GenScript, USA) was added to HA-*g*-C18 dissolved in cell culture media or PBS. The lipid film was then hydrated with the aqueous mixture of protein and HA-*g*-C18. Liposome diameters were measured using Zetasizer Nano ZS (Malvern Instrument Ltd.) equipped with a He–Ne laser beam at 633 nm (scattering angle: 173 °C). Each sample was measured three times, and an average diameter was obtained.

Analysis of Liposome on Cell Surface.

Adipose-derived stem cells (80 000 cells per group) were counted and suspended in cell culture media mixed with NBD-labeled liposomes. The cell density was kept constant at 10^6 cells mL^{-1}. The mixture was gently shaken at 37 °C for 15 min. After 15 min, the cells were

centrifuged and washed once with PBS. The mass of liposomes tethered to the cell surface was quantified by measuring the liposome mass in the supernatant using a black 96-well plate reader (TECAN Infinite M200 Pro; excitation wavelength: 460 nm, emission wavelength: 530 nm). Liposomes on the cell surface were also imaged using a confocal microscope (Zeiss LSM 700). Cells were fixed with 3.7% formaldehyde for 10 min before imaging. Confocal microscopy was carried out with excitation at 488 nm. Emission above 530 nm and bright-field images were collected.

Analysis of Secretion Activity of ADSCs.

Collagen hydrogels were prepared in a sterile condition. First, 200 μL of type I bovine collagen solution (3 mg mL^{-1} in 0.01 N hydrochloric acid; Advanced BioMatrix) was mixed with 100 μL of culture media. The mixture was pipetted without the formation of air bubbles until the phenol red changed to a homogeneous yellow color. Then, 25 μL of reconstituting solution (0.26 M sodium bicarbonate, 0.2 M HEPES, 0.04 N NaOH) was gently mixed with the collagen solution until the phenol red became pink. The pregel solution was quickly transferred to a precooled 96-well plate and incubated at 37 °C for 3 h.

To tether liposomes to the adipose-derived stem cells (Lonza), 160 000 ADSCs per group were counted and mixed with liposomes by gently shaking at 37 °C for 15 min. After 15 min, the cells were centrifuged (200*g*, 5 min) and resuspended in fresh media to a concentration of 100 000 cell mL^{-1}. Then, 100 μL of cell suspension was added to the premade collagen hydrogels. Cell culture media was collected after 24 h and 5 days.

A proteome profiler human angiogenesis array kit (R&D Systems, USA) was used to analyze the proteins in the cell culture media following the manufacturer's protocol. Briefly, 400 μL of cell culture supernatant was pooled ($n = 5$) and diluted with a cocktail of biotinylated antibodies. The mixture was then applied to a membrane precoated with multiple capture antibodies printed in duplicate. Samples were incubated at 4 °C overnight on a rotating shaker. Following multiple washes, a horseradish peroxidase-conjugated streptavidin conjugate was applied for 30 min. Blots were detected from the oxidation of luminol, and the emitted light was captured by exposure to X-ray films.

Separately, the amount of VEGF and PDEF were measured using a DuoSet enzyme-linked immunosorbent assay development system (R&D Systems, USA). Briefly, 96-well microplates were coated with the primary antibody diluted in PBS. The plates were incubated overnight at room temperature. Free binding sites were blocked with 0.1% bovine serum albumin in PBS. Samples or standards of 100 μL were added to each well. After incubation for 2 h at room temperature, biotinylated primary antibody was added, followed by addition of streptavidin/horseradish peroxidase. The plate was washed before each step with 0.05% Tween 20 in PBS. A substrate solution consisting of an equal mixture of Color Reagent A containing H_2O_2 and Color Reagent B containing tetramethylbenzidine (R&D Systems) was added and incubated for 20 min at room temperature. The reaction was stopped by the addition of 50 μL of 2 N H_2SO_4. The color intensity was measured immediately using a microplate reader (Tecan M200 Pro) set at 450 nm (with background correction wavelength set to 570 nm).

Microfluidic Chip Angiogenesis Assay.

A fibrinogen solution was prepared by dissolving 2.5 mg mL^{-1} bovine fibrinogen in Dulbecco's phosphate-buffered saline supplemented with aprotinin (0.15 U mL^{-1}, Sigma, A1153) to the solution. HUVECs (Lonza) and ADSCs were suspended in the fibrinogen solution, at a concentration of 2 to 3 × 10^6 cells mL^{-1} for HUVECs and 5 × 10^6 cells mL^{-1} for ADSCs. The HUVEC and ADSC suspensions were mixed with thrombin (0.5 U ml^{-1}) and then immediately introduced into the central and the two outer channels. The gels in these channels cross-linked within 5 min at room temperature. To fill the hydrophobic channels, the inlet reservoirs of the cell culture medium channels were loaded with culture medium, and the outlet reservoirs were connected to a vacuum source. The microfluidic platforms were incubated at 37 °C and 5% CO_2. The cell culture medium was removed and refilled with fresh culture medium every 24 h.

After 5 days, cells were washed once with PBS and fixed in a 4% (w/v) paraformaldehyde/PBS mixture for 15 min and then permeabilized using 0.15% Triton X-100 in PBS solution for 15 min. After blocking with 3% BSA in PBS for 1 h, the samples were incubated overnight at 4 °C with CD31 primary antibodies directly conjugated with fluorescent marker (1:200). The cell nuclei were stained with Hoechst 33342 (1:1000) for 1 h at room temperature. The chips were washed three times and stored in PBS before imaging. Quantification of tubule length was conducted using ImageJ software.

Induction of Ischemic Hindlimb Injury and Laser Doppler Perfusion Imaging Analysis.

The surgery to induce hindlimb ischemia was performed in accordance with the protocol approved by the Illinois Institutional Animal Care and Use Committee. The animals used were 7-week old female CD1 mice (Charles River). Under anesthesia, two sections of femoral artery, 2 mm apart, on the right limb were tied with 5–0 Ethilon sutures. Then, the middle section was cut before the surgical site was closed with 5–0 Ethilon sutures. ADSCs (1.0 × 10^6 cells per mouse) were suspended in 100 μL of PBS and injected intramuscularly at two sites (60 μL to the quadriceps and 40 μL to the tibialis anterior) using 28-gauge insulin syringes 1 h after the surgery. The overall perfusion recovery rate in the hindlimb was monitored by LDPI) of the whole leg after 1, 3, 7, 14, 21, and 28 days postcell transplantation. Prior to imaging, the fur on the legs and lower abdomen was shaved. Scans of the ischemic and nonischemic limbs were taken while the mice were placed on a 37 °C heating pad to control the body temperature. Seven or eight mice were analyzed per condition. On day 26, the stride length of recovering mice was measured using a previously described method.[47–49] The forepaws and hindpaws of the mice were dipped in green and red nontoxic inkpads, respectively. The mice were trained to walk along a 50-cm-long, 12-cm-wide, paper-covered runway. The stride length was determined by measuring the distance between two hindpaw prints.

Muscle Function and Histological Analysis.

The strength of the hindlimb muscles was assessed *in vivo* after 14 or 28 days. All mice were anesthetized with isoflurane (2–3% isoflurane, 0.9 L/min oxygen), and the hindlimb was aseptically prepared. Each mouse foot was placed on a miniature metal foot plate attached to the shaft of a servomotor (1300A, Aurora Scientific, Aurora, ON, Canada). The

foot was placed so that it was perpendicular to the tibia. Two platinum electrodes were inserted through the skin on either side of the sciatic nerve. A stimulator and stimulus unit activated the sciatic nerve *via* the platinum electrodes to induce contraction of the crural muscles to measure the maximal isometric force. The maximal force output was presented as torque from an individual mouse and normalized to the mass of the corresponding mouse. To assess the ability of the muscle to generate the maximal force after multiple contractions, the electrical stimulation was repeated for an additional nine times with 5 s recovery periods. Then, the muscle fatigue was represented by the percentage drop in muscle force. This was calculated by subtracting the value from the first stimulation from the last stimulation and dividing by the value from the first stimulation.

Immediately after the measurements, the mice were sacrificed, and the quadriceps, tibialis anterior, and gastrocnemius muscles were gently dissociated from underlying bone. Muscle weights were measured before they were immediately frozen in precooled isopentane. The frozen tissues were sectioned using a cryotome (Tissue-Tek; Fisher Scientific) and placed on microscope slides (Superfrost; Fisher Scientific). Then, sections were fixed in ice-cold acetone for 10 min and blocked with 5% BSA in serum.

Blood vessels in the muscle were identified by incubating the tissue section with rat monoclonal anti-CD31 (eBioscience), a marker for endothelial cells. Tissue sections were costained with mouse monoclonal antidystrophin (MANDRA1) (Sigma-Aldrich) to outline myofibers. Then, tissue sections were incubated with media dissolved with fluorescein isothiocyanate (FITC)-labeled donkey anti-rat (1:250) and rhodamine-labeled goat anti-mouse (1:100) secondary antibodies, which were used to identify the CD31 and dystrophin, respectively. Vascular density was quantified by counting the number of CD31-positive blood vessels in a unit area of dystrophin-positive myofibers.

To identify the arterioles, tissue sections were immunostained with mouse anti-α-smooth muscle actin (αSMA) FITC-conjugated antibody (1:100) (Sigma-Aldrich, F3777). By costaining with the vessel marker, CD31, αSMA-positive vessels were observed using ImageJ software (NIH), and αSMA-positive vessels smaller than 35 μm were counted as arterioles.

Statistical Analysis.

Three samples were analyzed per condition, and the data were presented as mean ± standard deviation unless otherwise specified. To determine significance, comparisons between groups were performed by one-way ANOVA followed by Tukey's *post hoc* analyses. Student's *t* tests with unequal or equal variance were used to compare differences between two experimental groups. Data were considered significant for p values less than 0.05.

Supplementary Material

Refer to Web version on PubMed Central for supplementary material.

ACKNOWLEDGMENTS

Dynamic light scattering was carried out in part in the Fredrick Seitz Materials Research Laboratory Central Facilities, University of Illinois. J.L. and J.Y.T. gratefully acknowledge the A*STAR Graduate Scholarship (Overseas) from the Agency for Science, Technology and Research (A*STAR) Singapore. Y.Y.Y. is grateful for the support from the Institute of Bioengineering and Nanotechnology (Biomedical Research Council, A*STAR, Singapore). Research reported in this publication was supported by the Korea Institute of Science and Technology (2E29340 to H.J.), National Institutes of Health (1R21 HL131469 to H.K. and M.B.), and National Institute of Biomedical Imaging and Bioengineering of the National Institutes of Health under (T32EB019944 to E.K.). The content is solely the responsibility of the authors and does not necessarily represent the official views of the National Institutes of Health.

REFERENCES

(1). Liew A; O'Brien T Therapeutic Potential for Mesenchymal Stem Cell Transplantation in Critical Limb Ischemia. Stem Cell Res. Ther 2012, 3, 28. [PubMed: 22846185]

(2). Tsuji W; Rubin JP; Marra KG Adipose-Derived Stem Cells: Implications in Tissue Regeneration. World J. Stem Cells 2014, 6, 312–321. [PubMed: 25126381]

(3). Wietecha MS; Król MJ; Michalczyk ER; Chen L; Gettins PG; DiPietro LA Pigment Epithelium-Derived Factor (PEDF) as a Multifunctional Regulator of Wound Healing. Am. J. Physiol.: Heart Circ. Physiol 2015, 309, H812–26. [PubMed: 26163443]

(4). Ito WD; Arras M; Winkler B; Scholz D; Schaper J; Schaper W Monocyte Chemotactic Protein-1 Increases Collateral and Peripheral Conductance after Femoral Artery Occlusion. Circ. Res 1997, 80, 829–837. [PubMed: 9168785]

(5). Spaggiari GM; Abdelrazik H; Becchetti F; Moretta L MSCs Inhibit Monocyte-Derived DC Maturation and Function by Selectively Interfering with the Generation of Immature DCs: Central Role of MSC-Derived Prostaglandin E2. Blood 2009, 113, 6576–6583. [PubMed: 19398717]

(6). Aggarwal S; Pittenger MF Human Mesenchymal Stem Cells Modulate Allogeneic Immune Cell Responses. Blood 2005, 105, 1815–1822. [PubMed: 15494428]

(7). Dopheide JF; Doppler C; Scheer M; Obst V; Radmacher MC; Radsak MP; Gori T; Warnholtz A; Fottner C; Münzel T; Daiber A; Espinola-Klein C Critical Limb Ischaemia Is Characterised by an Increased Production of Whole Blood Reactive Oxygen Species and Expression of TREM-1 on Neutrophils. Atherosclerosis 2013, 229, 396–403. [PubMed: 23880194]

(8). Lee SY; Kim W; Lim C; Chung SG Treatment of Lateral Epicondylosis by Using Allogeneic Adipose-Derived Mesenchymal Stem Cells: A Pilot Study. Stem Cells 2015, 33, 2995–3005. [PubMed: 26202898]

(9). Toyserkani NM; Jørgensen MG; Tabatabaeifar S; Jensen CH; Sheikh SP; Sørensen JA Concise Review: A Safety Assessment of Adipose-Derived Cell Therapy in Clinical Trials: A Systematic Review of Reported Adverse Events. Stem Cells Transl. Med 2017, 6, 1786–1794. [PubMed: 28722289]

(10). Ankrum JA; Ong JF; Karp JM Mesenchymal Stem Cells: Immune Evasive, Not Immune Privileged. Nat. Biotechnol 2014, 32, 252–260. [PubMed: 24561556]

(11). Iseri K; Iyoda M; Ohtaki H; Matsumoto K; Wada Y; Suzuki T; Yamamoto Y; Saito T; Hihara K; Tachibana S; Honda K; Shibbata T Therapeutic Effects and Mechanism of Conditioned Media from Human Mesenchymal Stem Cells on Anti-GBM Glomerulonephritis in WKY Rats. Am. J. Physiol.: Renal Physiol 2016, 310, F1182–91. [PubMed: 27053690]

(12). Herrmann JL; Wang Y; Abarbanell AM; Weil BR; Tan J; Meldrum DR Preconditioning Mesenchymal Stem Cells with Transforming Growth Factor-Alpha Improves Mesenchymal Stem Cell-Mediated Cardioprotection. Shock 2010, 33, 24–30. [PubMed: 19996917]

(13). Xu B; Luo Y; Liu Y; Li B; Wang Y Platelet-Derived Growth Factor-BB Enhances MSC-Mediated Cardioprotection *via* Suppression of MiR-320 Expression. Am. J. Physiol.: Heart Circ. Physiol 2015, 308, H980–H989. [PubMed: 25724494]

(14). Zubkova ES; Beloglazova IB; Makarevich PI; Boldyreva MA; Sukhareva OY; Shestakova MV; Dergilev KV; Parfyonova YV; Menshikov MY Regulation of Adipose Tissue Stem Cells

Angiogenic Potential by Tumor Necrosis Factor-Alpha. J. Cell. Biochem 2016, 117, 180–196. [PubMed: 26096299]

(15). Ranganath SH; Levy O; Inamdar MS; Karp JM Harnessing the Mesenchymal Stem Cell Secretome for the Treatment of Cardiovascular Disease. Cell Stem Cell 2012, 10, 244–258. [PubMed: 22385653]

(16). Ankrum JA; Dastidar RG; Ong JF; Levy O; Karp JM Performance-Enhanced Mesenchymal Stem Cells *via* Intracellular Delivery of Steroids. Sci. Rep 2015, 4, 4645.

(17). Martinez VG; Ontoria-Oviedo I; Ricardo CP; Harding SE; Sacedon R; Varas A; Zapata A; Sepulveda P; Vicente A Overexpression of Hypoxia-Inducible Factor 1 Alpha Improves Immunomodulation by Dental Mesenchymal Stem Cells. Stem Cell Res. Ther 2017, 8, 208. [PubMed: 28962641]

(18). Lu W; Chen X; Si Y; Hong S; Shi Z; Fu W Transplantation of Rat Mesenchymal Stem Cells Overexpressing Hypoxia-Inducible Factor 2 α Improves Blood Perfusion and Arteriogenesis in a Rat Hindlimb Ischemia Model. Stem Cells Int. 2017, 2017, 1–11.

(19). Haider HK; Jiang S; Idris NM; Ashraf M IGF-1-Overexpressing Mesenchymal Stem Cells Accelerate Bone Marrow Stem Cell Mobilization *via* Paracrine Activation of SDF-1α/CXCR4 Signaling to Promote Myocardial Repair. Circ. Res 2008, 103, 1300–1308. [PubMed: 18948617]

(20). Oikonomopoulos A; Van Deen WK; Manansala AR; Lacey PN; Tomakili TA; Ziman A; Hommes DW Optimization of Human Mesenchymal Stem Cell Manufacturing: The Effects of Animal/Xeno-Free Media. Sci. Rep 2015, 5, 16570. [PubMed: 26564250]

(21). Choi MR; Kim HY; Park JY; Lee TY; Baik CS; Chai YG; Jung KH; Park KS; Roh W; Kim KS; Kim SH Selection of Optimal Passage of Bone Marrow-Derived Mesenchymal Stem Cells for Stem Cell Therapy in Patients with Amyotrophic Lateral Sclerosis. Neurosci. Lett 2010, 472, 94–98. [PubMed: 20117176]

(22). Pal R; Hanwate M; Jan M; Totey S Phenotypic and Functional Comparison of Optimum Culture Conditions for Upscaling of Bone Marrow-Derived Mesenchymal Stem Cells. J. Tissue Eng. Regener. Med 2009, 3, 163–174.

(23). Gregory CA; Ylostalo J; Prockop DJ Adult Bone Marrow Stem/Progenitor Cells (MSCs) Are Preconditioned by Micro-environmental "Niches" in Culture: A Two-Stage Hypothesis for Regulation of MSC Fate. Sci. Signaling 2005, 2005, pe37.

(24). Lee MJ; Kim J; Kim MY; Bae YS; Ryu SH; Lee TG; Kim JH Proteomic Analysis of Tumor Necrosis Factor-α-Induced Secretome of Human Adipose Tissue-Derived Mesenchymal Stem Cells. J. Proteome Res 2010, 9, 1754–1762. [PubMed: 20184379]

(25). Li X; Shang B; Li YN; Shi Y; Shao C IFNγ and TNFα Synergistically Induce Apoptosis of Mesenchymal Stem/Stromal Cells *via* the Induction of Nitric Oxide. Stem Cell Res. Ther 2019, 10, 1–11. [PubMed: 30606242]

(26). Zhu H; Mitsuhashi N; Klein A; Barsky LW; Weinberg K; Barr ML; Demetriou A; Wu GD The Role of the Hyaluronan Receptor CD44 in Mesenchymal Stem Cell Migration in the Extracellular Matrix. Stem Cells 2006, 24, 928–935. [PubMed: 16306150]

(27). Takahashi R; Kubota K; Kawada M; Okamoto A Effect of Molecular Weight Distribution on the Solution Properties of Sodium Hyaluronate in 0.2M NaCl Solution. Biopolymers 1999, 50, 87–98.

(28). Mizrahy S; Raz SR; Hasgaard M; Liu H; Soffer-Tsur N; Cohen K; Dvash R; Landsman-Milo D; Bremer MGEG; Moghimi SM; Peer D Hyaluronan-Coated Nanoparticles: The Influence of the Molecular Weight on CD44-Hyaluronan Interactions and on the Immune Response. J. Controlled Release 2011, 156, 231–238.

(29). Wolny PM; Banerji S; Gounou C; Brisson AR; Day AJ; Jackson DG; Richter RP Analysis of CD44-Hyaluronan Interactions in an Artificial Membrane System: Insights into the Distinct Binding Properties of High and Low Molecular Weight Hyaluronan. J. Biol. Chem 2010, 285, 30170–30180. [PubMed: 20663884]

(30). Ritger PL; Peppas NA A Simple Equation for Description of Solute Release I. Fickian and Non-Fickian Release from Non-Swellable Devices in the Form of Slabs, Spheres, Cylinders or Discs. J. Controlled Release 1987, 5, 23–36.

(31). Cheng H; Byrska-Bishop M; Zhang CT; Kastrup CJ; Hwang NS; Tai AK; Lee WW; Xu X; Nahrendorf M; Langer R; Anderson DG Stem Cell Membrane Engineering for Cell Rolling Using Peptide Conjugation and Tuning of Cell-Selectin Interaction Kinetics. Biomaterials 2012, 33, 5004–5012. [PubMed: 22494889]

(32). Park J; Andrade B; Seo Y; Kim M-J; Zimmerman SC; Kong H Engineering the Surface of Therapeutic “Living” Cells. Chem. Rev 2018, 118, 1664–1690. [PubMed: 29336552]

(33). Gordon S Phagocytosis: An Immunobiologic Process. Immunity 2016, 44, 463–475. [PubMed: 26982354]

(34). Schäfer R; Spohn G; Baer PC Mesenchymal Stem/Stromal Cells in Regenerative Medicine: Can Preconditioning Strategies Improve Therapeutic Efficacy? Transfus. Med. Hemotherapy 2016, 43, 256–267.

(35). Doorn J; Moll G; Le Blanc K; van Blitterswijk C; de Boer J Therapeutic Applications of Mesenchymal Stromal Cells: Paracrine Effects and Potential Improvements. Tissue Eng., Part B 2012, 18, 101–115.

(36). Tang L; Zheng Y; Melo MB; Mabardi L; Castaño AP; Xie YQ; Li N; Kudchodkar SB; Wong HC; Jeng EK; Maus MV; Irvine DJ Enhancing T Cell Therapy through TCR-Signaling-Responsive Nanoparticle Drug Delivery. Nat. Biotechnol 2018, 36, 707–716. [PubMed: 29985479]

(37). Han Q; Bagheri N; Bradshaw EM; Hafler DA; Lauffenburger DA; Love JC Polyfunctional Responses by Human T Cells Result from Sequential Release of Cytokines. Proc. Natl. Acad. Sci. U. S. A 2012, 109, 1607–1612. [PubMed: 22160692]

(38). Thurley K; Gerecht D; Friedmann E; Höfer T Three-Dimensional Gradients of Cytokine Signaling between T Cells. PLoS Comput. Biol 2015, 11, No. e1004206. [PubMed: 25923703]

(39). Kumari S; Mg S; Mayor S Endocytosis Unplugged: Multiple Ways to Enter the Cell. Cell Res. 2010, 20, 256–275. [PubMed: 20125123]

(40). Rajashekhar G; Kamocka M; Marin A; Suckow MA; Wolter WR; Badve S; Sanjeevaiah AR; Pumiglia K; Rosen E; Clauss M Pro-Inflammatory Angiogenesis Is Mediated by P38 MAP Kinase. J. Cell. Physiol 2011, 226, 800–808. [PubMed: 20803566]

(41). Tomida T; Takekawa M; Saito H Oscillation of P38 Activity Controls Efficient Pro-Inflammatory Gene Expression. Nat. Commun 2015, 6, 1–9.

(42). Sarojini H; Estrada R; Lu H; Dekova S; Lee MJ; Gray RD; Wang E PEDF from Mouse Mesenchymal Stem Cell Secretome Attracts Fibroblasts. J. Cell. Biochem 2008, 104, 1793–1802. [PubMed: 18348263]

(43). Yañez R; Oviedo A; Aldea M; Bueren JA; Lamana ML Prostaglandin E2 Plays a Key Role in the Immunosuppressive Properties of Adipose and Bone Marrow Tissue-Derived Mesenchymal Stromal Cells. Exp. Cell Res 2010, 316, 3109–3123. [PubMed: 20804749]

(44). Shin Y; Han S; Jeon JS; Yamamoto K; Zervantonakis IK; Sudo R; Kamm RD; Chung S Microfluidic Assay for Simultaneous Culture of Multiple Cell Types on Surfaces or within Hydrogels. Nat. Protoc 2012, 7, 1247–1259. [PubMed: 22678430]

(45). Helisch A; Wagner S; Khan N; Drinane M; Wolfram S; Heil M; Ziegelhoeffer T; Brandt U; Pearlman JD; Swartz HM; Schaper W Impact of Mouse Strain Differences in Innate Hindlimb Collateral Vasculature. Arterioscler., Thromb., Vasc. Biol 2006, 26, 520–526. [PubMed: 16397137]

(46). Shireman PK; Contreras-Shannon V; Ochoa O; Karia BP; Michalek JE; McManus LM MCP-1 Deficiency Causes Altered Inflammation with Impaired Skeletal Muscle Regeneration. J. Leukocyte Biol 2007, 81, 775–785. [PubMed: 17135576]

(47). Girirajan S; Patel N; Slager RE; Tokarz MEME; Bucan M; Wiley JL; Elsea SH How Much Is Too Much? Phenotypic Consequences of Rai1 Overexpression in Mice. Eur. J. Hum. Genet 2008, 16, 941–954. [PubMed: 18285828]

(48). Wang H; Chen X; Li Y; Tang TS; Bezprozvanny I Tetrabenazine Is Neuroprotective in Huntington’s Disease Mice. Mol. Neurodegener 2010, 5, 18. [PubMed: 20420689]

(49). Fernagut PO; Diguet E; Labattu B; Tison F A Simple Method to Measure Stride Length as an Index of Nigrostriatal Dysfunction in Mice. J. Neurosci. Methods 2002, 113, 123–130. [PubMed: 11772434]

(50). Semenza GL Vasculogenesis, Angiogenesis, and Arterio-genesis: Mechanisms of Blood Vessel Formation and Remodeling. J. Cell. Biochem 2007, 102, 840–847. [PubMed: 17891779]

(51). Borselli C; Storrie H; Benesch-Lee F; Shvartsman D; Cezar C; Lichtman JW; Vandenburgh HH; Mooney DJ Functional Muscle Regeneration with Combined Delivery of Angiogenesis and Myogenesis Factors. Proc. Natl. Acad. Sci. U. S. A 2010, 107, 3287–3292. [PubMed: 19966309]

(52). Anderson EM; Kwee BJ; Lewin SA; Raimondo T; Mehta M; Mooney DJ Local Delivery of VEGF and SDF Enhances Endothelial Progenitor Cell Recruitment and Resultant Recovery from Ischemia. Tissue Eng., Part A 2015, 21, 1217–1227. [PubMed: 25434326]

(53). Zhao L; Huang J; Zhang H; Wang Y; Matesic LE; Takahata M; Awad H; Chen D; Xing L Tumor Necrosis Factor Inhibits Mesenchymal Stem Cell Differentiation into Osteoblasts *via* the Ubiquitin E3 Ligase Wwp1. Stem Cells 2011, 29, 1601–1610. [PubMed: 21809421]

(54). Lotfi S; Patel AS; Mattock K; Egginton S; Smith A; Modarai B Towards a More Relevant Hind Limb Model of Muscle Ischaemia. Atherosclerosis 2013, 227, 1–8. [PubMed: 23177969]

(55). Hudlicka O; Brown MD; Egginton S; Dawson JM Effect of Long-Term Electrical Stimulation on Vascular Supply and Fatigue in Chronically Ischemic Muscles. J. Appl. Physiol 2017, 77, 1317–1324.

(56). Chen M; Fan H; Ledford BT; Farah Z; Barron C; Liu Z; He JQ Impacts of Femoral Artery and Vein Excision *versus* Femoral Artery Excision on the Hindlimb Ischemic Model in CD-1 Mice. Microvasc. Res 2017, 110, 48–55. [PubMed: 27998712]

(57). Dragneva G; Korpisalo P; Ylä-Herttuala S Promoting Blood Vessel Growth in Ischemic Diseases: Challenges in Translating Preclinical Potential into Clinical Success. Dis. Models & Mech 2013, 6, 312–322.

(58). Kim H; Han JW; Lee JY; Choi YJ; Sohn YD; Song M; Yoon YS Diabetic Mesenchymal Stem Cells Are Ineffective for Improving Limb Ischemia Due to Their Impaired Angiogenic Capability. Cell Transplant 2015, 24, 1571–1584. [PubMed: 25008576]

(59). Yan J; Tie G; Park B; Yan Y; Nowicki PT; Messina LM Recovery from Hind Limb Ischemia Is Less Effective in Type 2 Than in Type 1 Diabetic Mice: Roles of Endothelial Nitric Oxide Synthase and Endothelial Progenitor Cells. J. Vasc. Surg 2009, 50, 1412–1422. [PubMed: 19837544]

(60). Westvik TS; Fitzgerald TN; Muto A; Maloney SP; Pimiento JM; Fancher TT; Magri D; Westvik HH; Nishibe T; Velazquez OC; Dardik A Limb Ischemia after Iliac Ligation in Aged Mice Stimulates Angiogenesis without Arteriogenesis. J. Vasc. Surg 2009, 49, 464–473. [PubMed: 19028053]

(61). Center for Biologics Evaluation and Research. Regulatory Considerations for Human Cells, Tissues, and Cellular and Tissue-Based Products: Minimal Manipulation and Homologous Use; FDA-2017-D-6146; U.S. Food and Drug Administration: Silver Spring, MD, 2017; pp 1–24.

(62). Misra S; Hascall VC; Markwald RR; Ghatak S Interactions between Hyaluronan and Its Receptors (CD44, RHAMM) Regulate the Activities of Inflammation and Cancer. Front. Immunol 2015, 6, 201. [PubMed: 25999946]

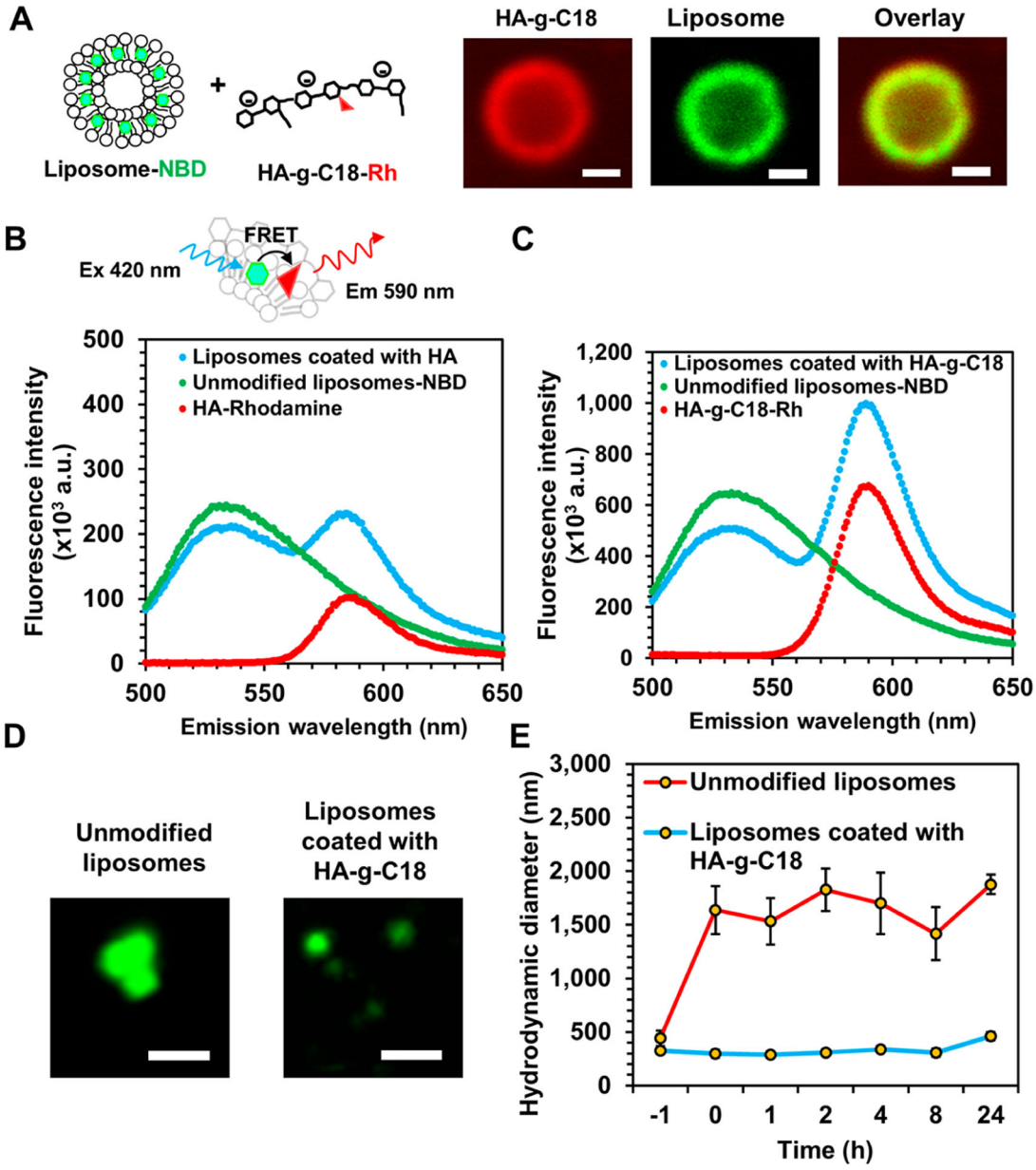

Figure 1.

Physical characterization of liposomes coated with hyaluronic acid-*g*-C18 (HA-*g*-C18). (A) Fluorescence images of liposomes coated with HA-*g*-C18 where HA-*g*-C18 were labeled with rhodamine B (Rh in red) and the lipid layer was labeled with nitrobenzoxadiazole (NBD) (in green). Lipids were covalently bound to NBD. The overlay panel shows the merged images. Images were taken after mixing HA-*g*-C18 and liposomes at a mass ratio of 2:1. Scale bars represent 1 μm. (B) Förster resonance energy transfer (FRET) assay to evaluate the association between HA-*g*-C18 and liposomes or (C) unmodified HA and liposomes. All three samples were excited at wavelength of 460 nm. (D) Fluorescence images of unmodified liposomes and liposomes coated with HA-*g*-C18 incubated in media supplemented with 10% serum. Scale bar represents 1 μm. (E) Hydrodynamic diameter of

liposomes with (in blue) and without HA-*g*-C18 (in red) incubated in media supplemented with 10% serum at 37 °C. Data points represent the mean, and error bars represent standard deviations. $N = 3$.

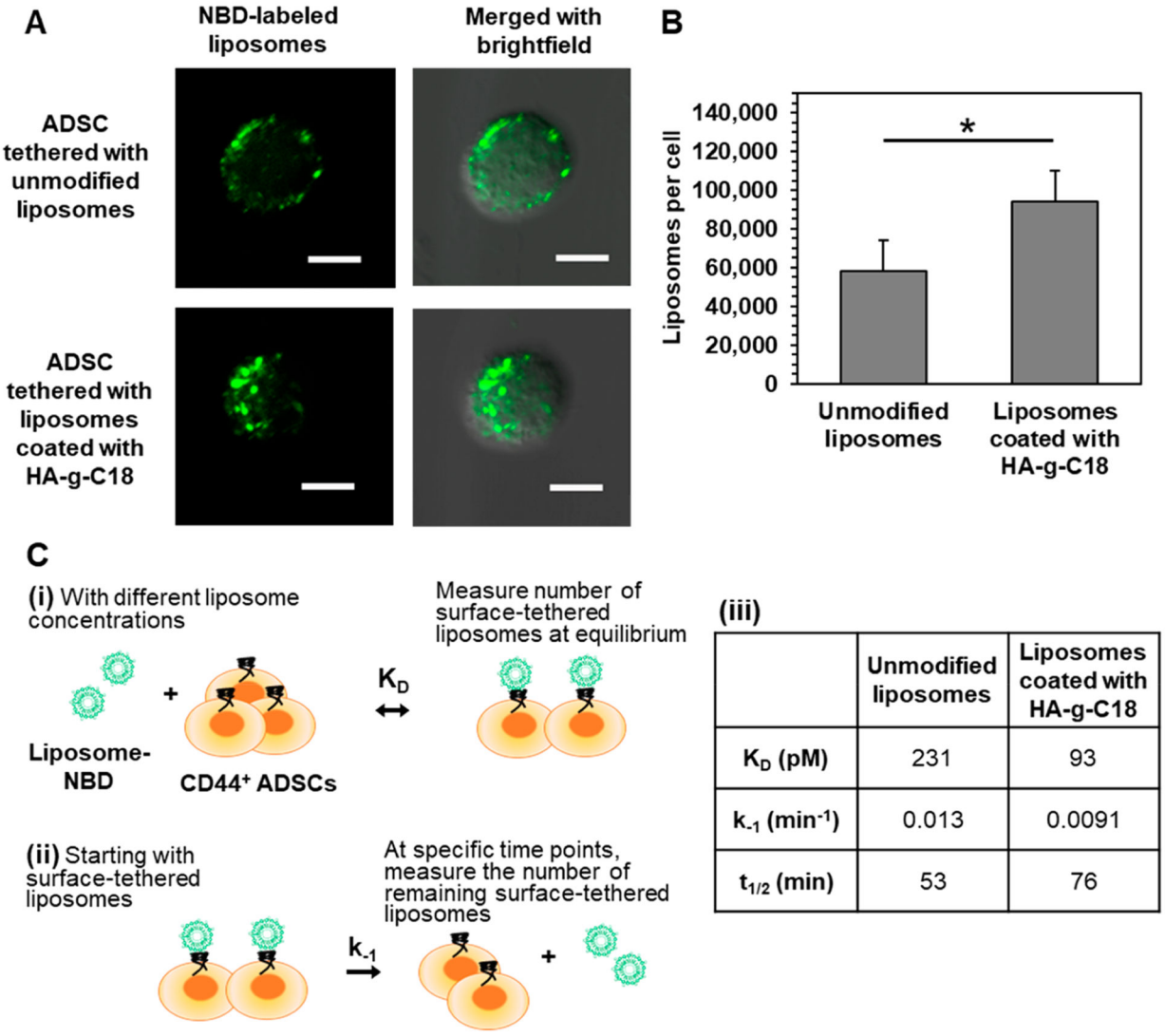

	Unmodified liposomes	Liposomes coated with HA-g-C18
K_D (pM)	231	93
k_{-1} (min^{-1})	0.013	0.0091
$t_{1/2}$ (min)	53	76

Figure 2.

Characterization of the association of liposomes with ADSCs. (A) Confocal microscope images of ADSCs after incubation with unmodified liposomes or liposomes coated with HA-*g*-C18. Liposomes were fluorescently labeled using the covalently bound NBD fluorophore (in green). Scale bar represents 10 μm. (B) Quantification of the number of liposomes on the surface of ADSCs. Data points represent the mean, and error bars represent standard deviations. $N = 3$, * represents the statistical significance in the number of liposomes between the unmodified liposomes and liposomes coated with HA-*g*-C18. *$p < 0.05$. (C) Schematic illustration of the kinetic analysis of the liposome tethering to ADSCs. (i) At a given liposome concentration, the number of liposomes tethered to cells was measured to quantify the dissociation equilibrium constant, K_D. (ii) The dissociation rate constant, k_{-1}, the half-time of liposome dissociation, $t_{1/2}$, and the number of remaining surface-tethered liposomes were measured by counting the liposomes detached from cells at different time points. (iii) Tabulation of K_D, k_{-1}, and $t_{1/2}$ of unmodified liposomes and liposomes coated with HA-*g*-C18.

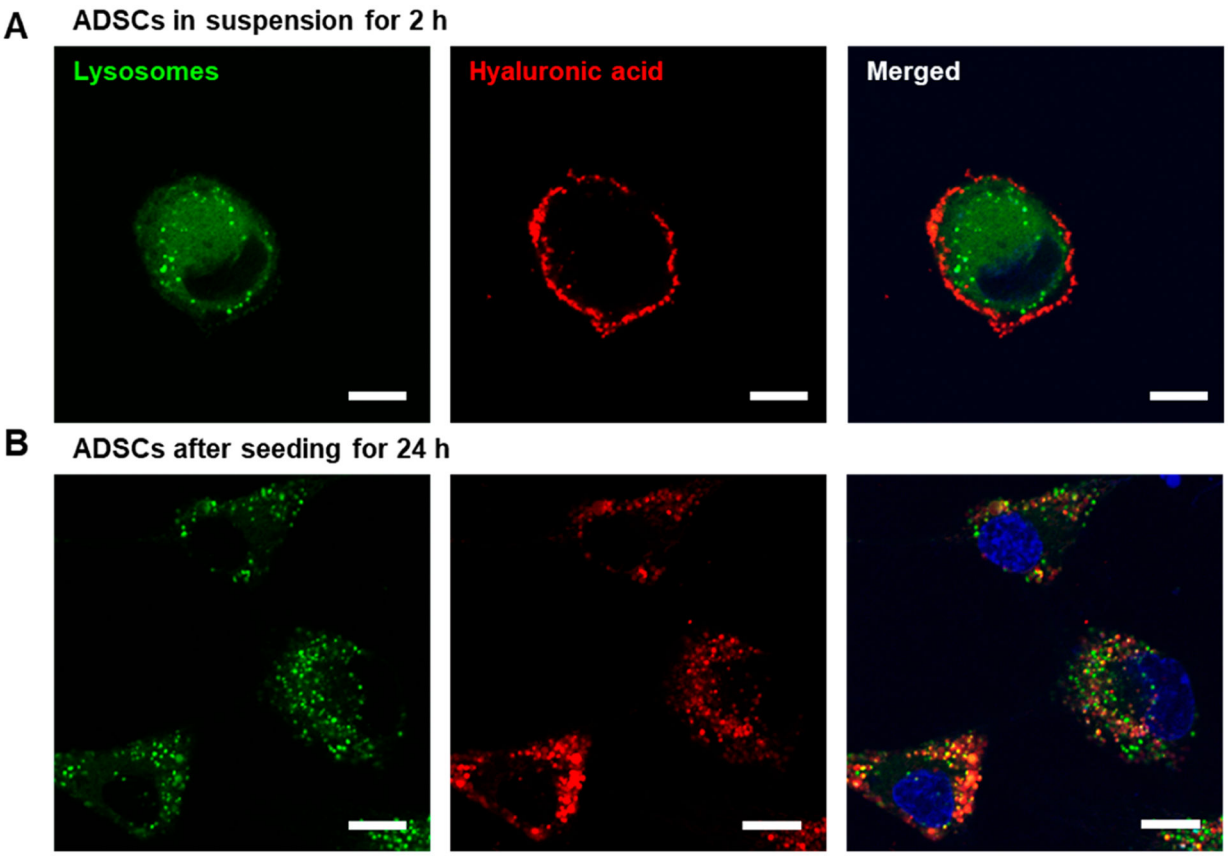

Figure 3.

Confocal microscope analysis to determine cellular internalization of liposomes coated with HA-*g*-C18. Lysosomes were labeled with LysoTracker Green, while liposomes were labeled with rhodamine B-conjugated HA-*g*-C18 (red). (A) ADSCs were incubated in suspension for 2 h. (B) ADSCs were incubated on type I collagen hydrogels for 24 h. The third column shows the merged images of the first two columns. Scale bars represent 10 μm.

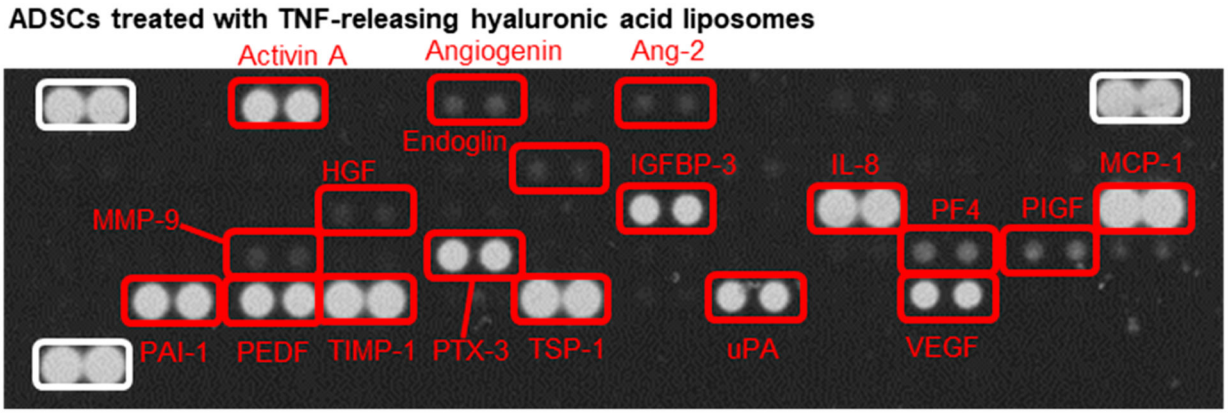

Figure 4.

Analysis of the secretory activity of ADSCs using the angiogenesis antibody array. Images of angiogenesis antibody array membrane incubated with media from the ADSC culture after 24 h. ADSCs tethered with TNFα-releasing HA-liposomes secrete growth factors and cytokines involved in proangiogenesis, antiangiogenesis, fibrosis, antiapoptosis, and tissue remodeling.

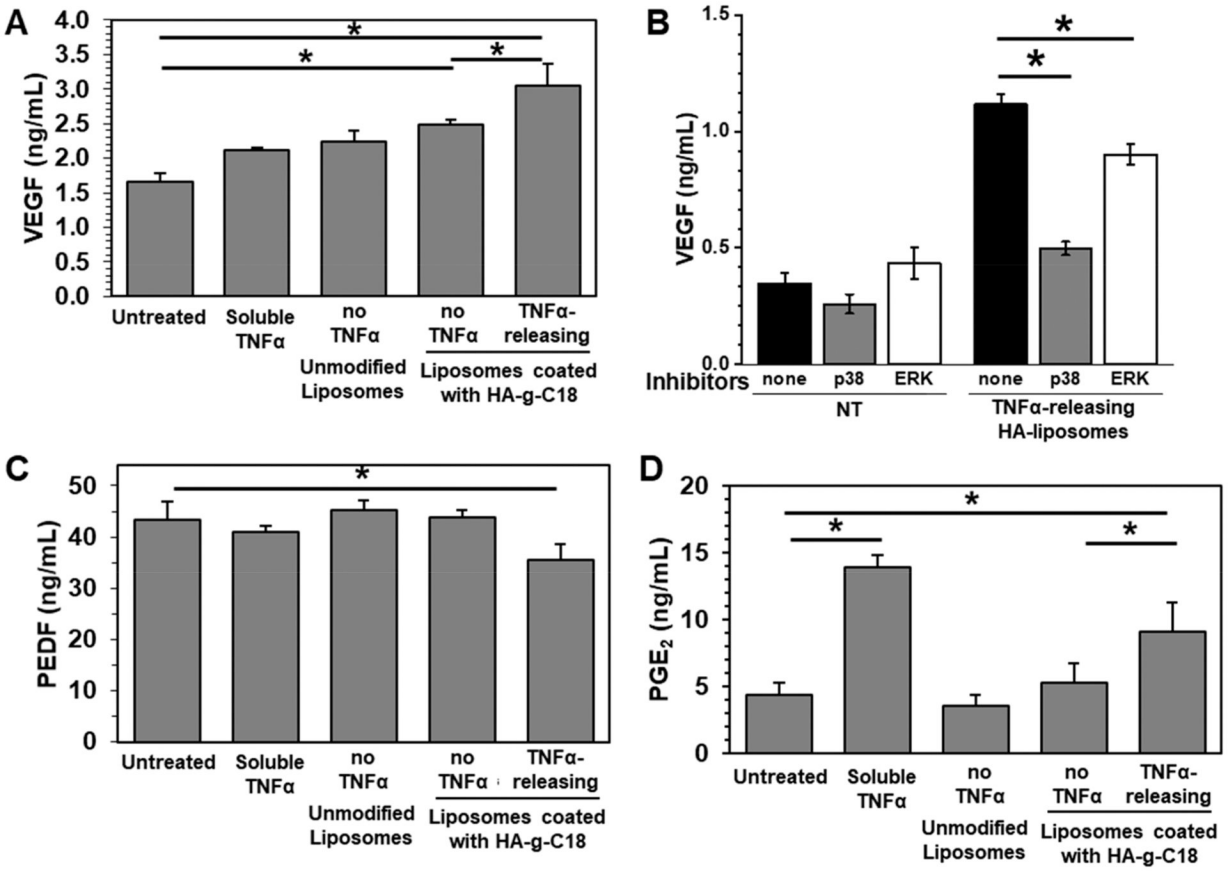

Figure 5.

Quantification of proangiogenic VEGF, antiangiogenic PEDF, and immunomodulatory PGE_2 levels secreted by ADSCs using ELISA. (A) VEGF secretion level. (B) Amount of VEGF in the media cultured with untreated ADSCs and ADSCs tethered with TNFα-releasing HA-liposomes after 24 h of incubation in the absence or presence of p38 MAPK or ERK inhibitors. (C) PEDF secretion level and (D) PGE_2 secretion level. Data points represent the mean and error bars represent standard deviations. $N = 3$, * represents the statistical significance between the conditions indicated. $*p < 0.05$.

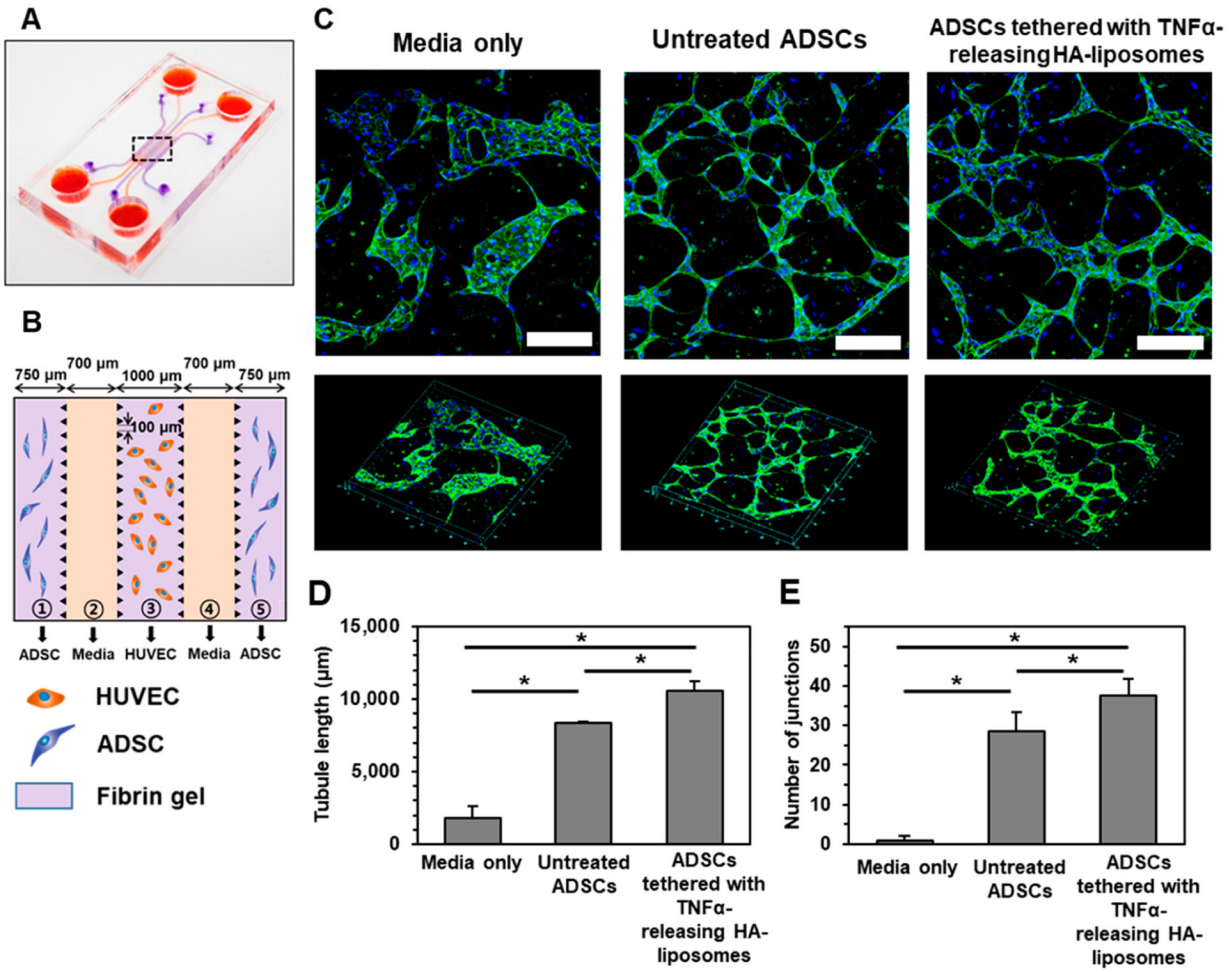

Figure 6.

In vitro angiogenesis assay with a 3D microvascular device. (A) Schematic illustration of the device fabricated with polydimethylsiloxane using soft lithography. (B) The central portion features five channels. ADSCs in fibrin gels were seeded in the outer channels ① and ⑤; cell culture medium was filled in channels ② and ④; and HUVECs in the fibrin gel were seeded in the center channel ③. (C) Confocal laser scanning microscope images of immunostained HUVECs with CD31 (in green) in channel ③ after 5 days of incubation with the cell culture media only, with untreated ADSCs only, or ADSCs tethered with TNFα-releasing HA-liposomes. Cell nuclei were stained with Hoechst dye (in blue). Scale bar represents 200 μm. The lower panels display an overview of the selected region. (D) Quantification of the tubule length and (E) the number of interconnected junctions. Data points represent the mean, and error bars represent standard deviations. $N = 3$, * represents the statistical significant between the conditions indicated. *$p < 0.05$.

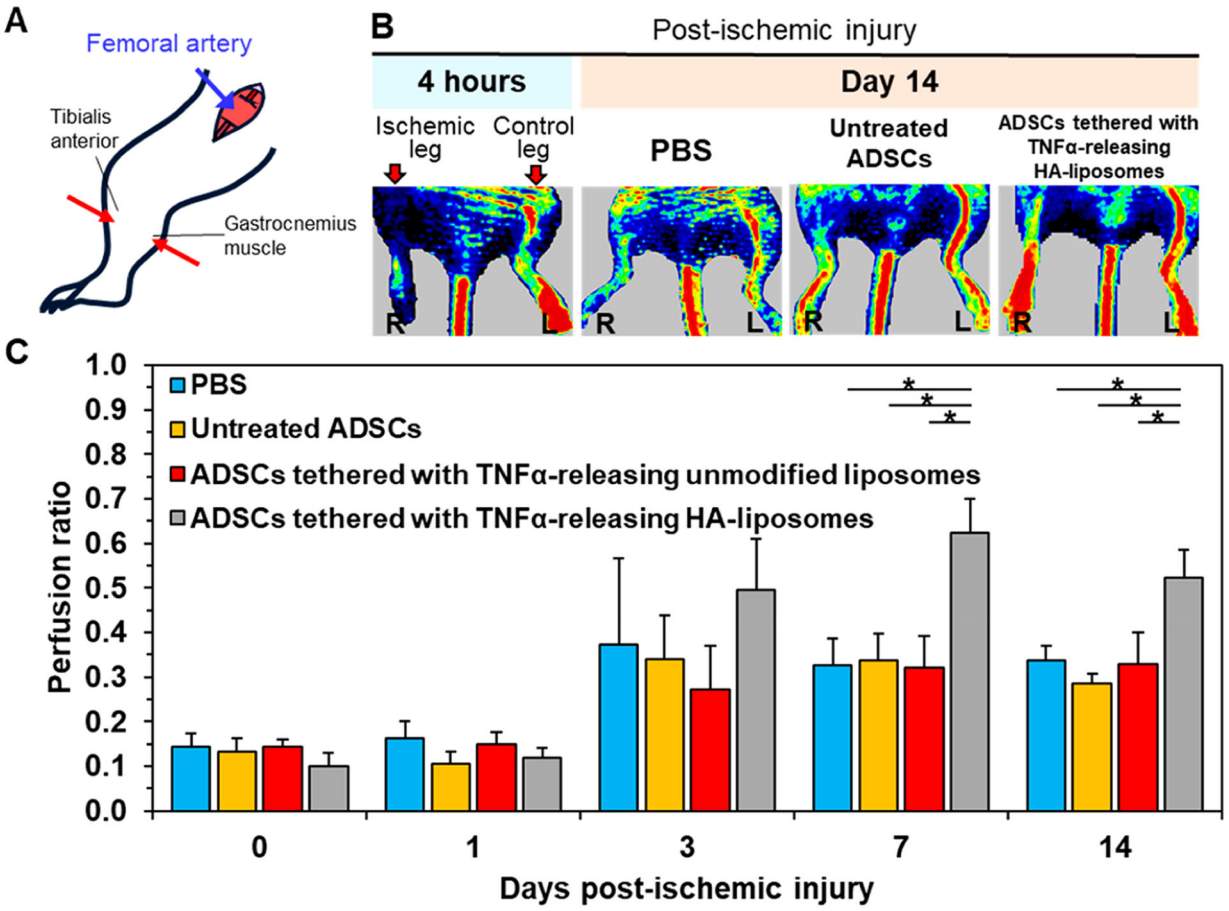

Figure 7.

Laser Doppler perfusion imaging of mice induced with ischemic hindlimb injury. (A) Schematic diagram of the surgery to induce limb ischemia followed by cell injection into the limb. (B) LDPI images of mice after the ischemic hindlimb surgery. Ischemia was introduced by ligating the femoral artery in the right leg. The color scale represents the relative intensity of perfusion with red representing the highest intensity. The ischemic leg imaged after 24 h and after it was treated for 14 days with 1 million ADSCs, 1 million untreated ADSCs, and 1 million ADSCs tethered with TNFα-releasing HA-liposomes. (C) Quantification of the mean perfusion ratio defined as the perfusion in the ischemic limb divided by the perfusion in the nonischemic limb ($N = 7$ mice, $^*p < 0.05$).

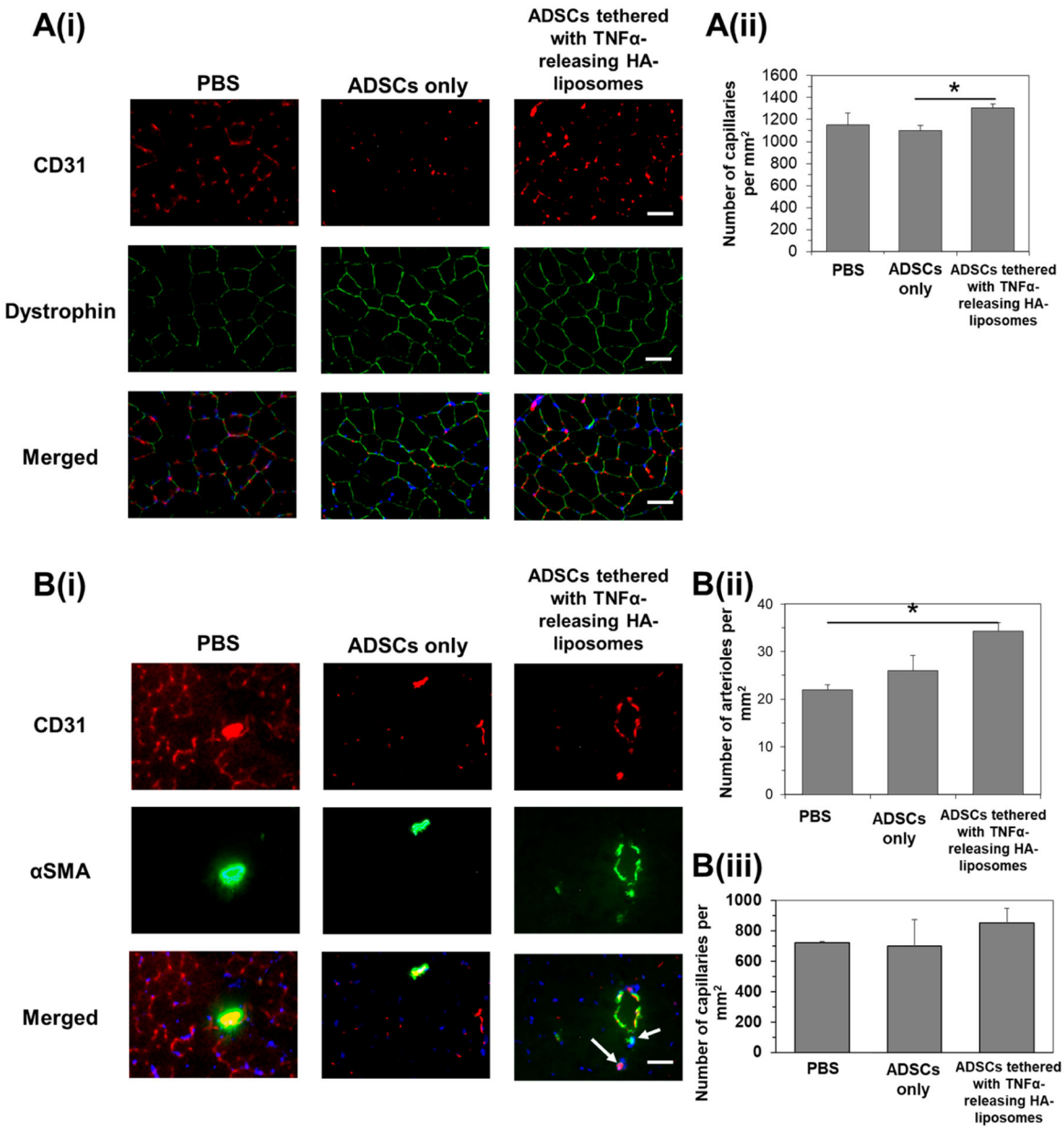

Figure 8.

Immunohistological analysis of muscle tissues 14 days after ischemic injury and injection of ADSCs only or ADSCs tethered with TNFα-releasing HA liposomes. (A(i)) The tibialis anterior muscle was stained with antibodies against CD31 (in red) and dystrophin (in green). Merged images on the bottom row show cell nuclei (in blue), CD31 (in red), and dystrophin (in green). Scale bar represents 50 μm. (A(ii)) Quantification of the capillary density in the tibialis anterior. * represents significant difference between the two groups, *$p < 0.05$. (B(i)) The gastrocnemius muscle was stained with antibodies against CD31 (in red) and alpha smooth muscle actin (αSMA, in green). Merged images on the bottom row show cell nuclei (in blue), CD31 (in red), and αSMA (in green). White arrows point to smaller arterioles. Scale bar represents 50 μm. Quantification of the (ii) total arteriole and (iii) capillary density

in the gastrocnemius muscle. * represents significant difference between the two groups, *$p < 0.05$.

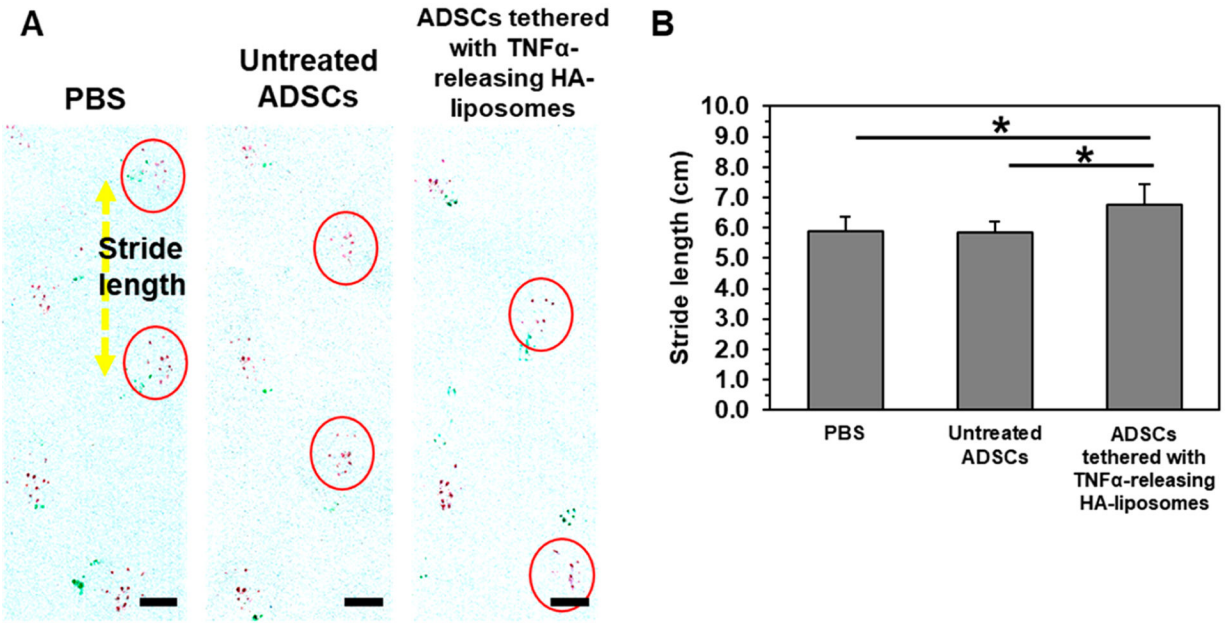

Figure 9.

Gait analysis of recovered mice on day 26. (A) Footpads of mice, forepaws and hindpaws, were dipped in green and red inkpads, respectively. Images were treated for higher image contrast of the red ink. Scale bar represents 2 cm. (B) Quantification of the average stride length ($N = 7$, 8 mice, $*p < 0.05$).

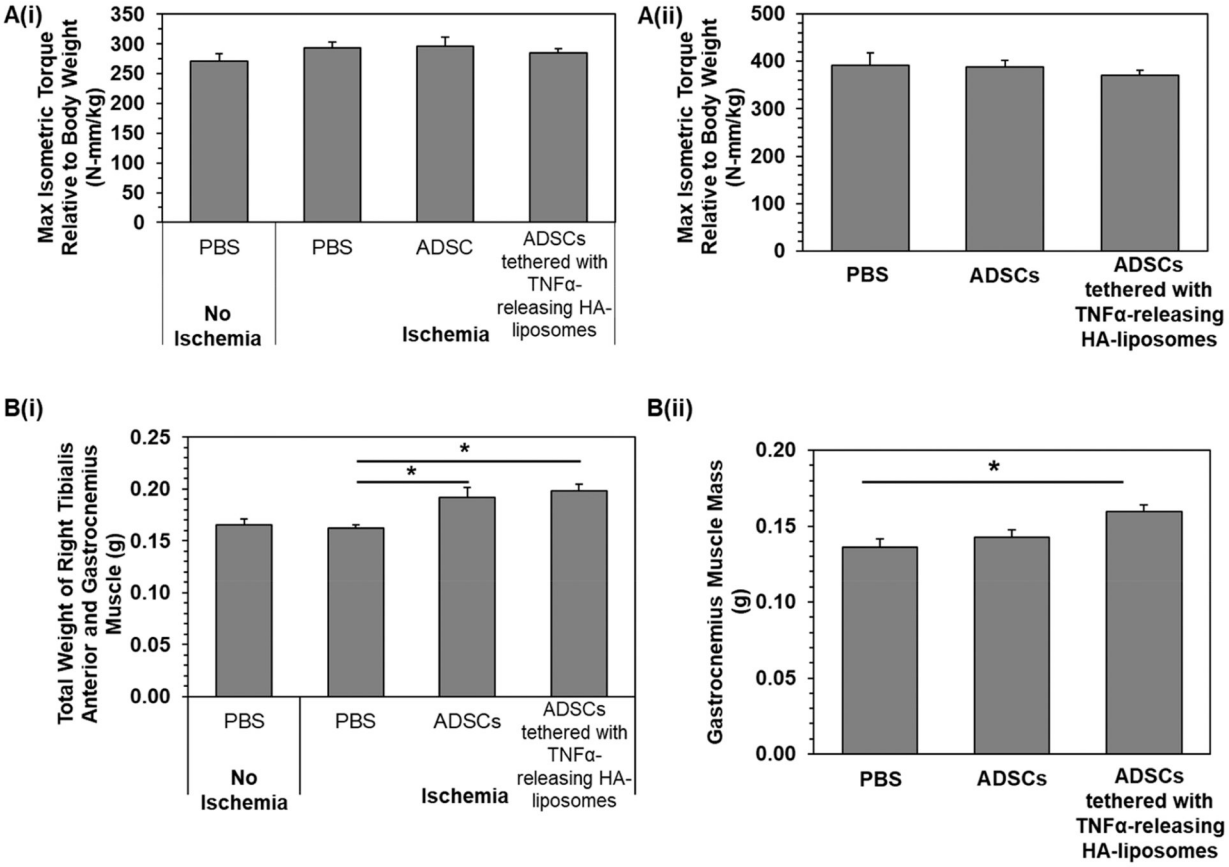

Figure 10.

Muscle force measurements of recovered mice at the end points, (i) day 14 and (ii) day 28, respectively. (A) Maximum isometric torque relative to body weight was determined by measuring the muscle force and dividing it by the mouse body weight. (B) Weight of the right muscles, tibialis anterior and gastrocnemius muscle. Bars represent the average value, and error bars indicate standard error. * represents significant difference between the two groups, $*p < 0.05$ ($N = 7, 8$).

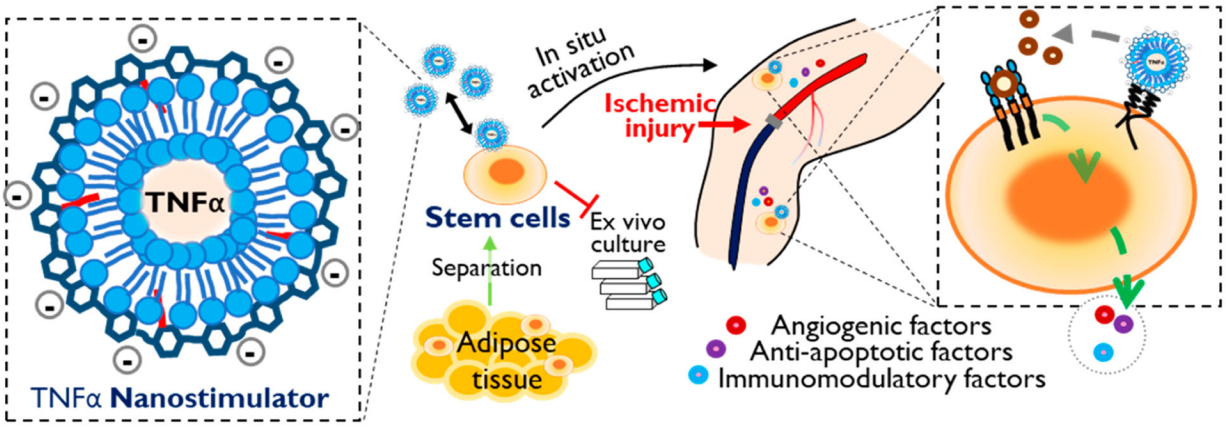

Scheme 1.

In situ stimulation of adipose-derived stem cells (ADSCs) for cellular therapy in ischemic tissue recovery. Nanostimulator consists of a TNFα-releasing liposome coated with hyaluronic acid-graft-octadecylamine (HA-g-C18). HA drives the liposomes tethered to the stem cell surface *via* specific binding with CD44. The nanostimulator on the stem cell surface up-regulates cellular secretion levels of angiogenic and immunomodulatory factors for revascularization and the prevention of muscle damage. Also, the nanostimulator removes *ex vivo* culture for pre-conditioning of stem cells, thus allowing for isolation and injection in an operating room.